PHYSICAL REVIEW B **92**, 245108 (2015)

Ab initio downfolding for electron-phonon-coupled systems: Constrained density-functional perturbation theory

Yusuke Nomura[1,*] and Ryotaro Arita[2,3]

[1]*Department of Applied Physics, University of Tokyo, Hongo, Bunkyo-ku, Tokyo 113-8656, Japan*

[2]*Center for Emergent Matter Science (CEMS), RIKEN, Hirosawa, Wako, Saitama 351-0198, Japan*

[3]*JST ERATO Isobe Degenerate π-Integration Project, AIMR, Tohoku University, 2-1-1 Katahira, Aoba-ku, Sendai 980-8577, Japan*

(Received 20 August 2015; published 7 December 2015)

We formulate an *ab initio* downfolding scheme for electron-phonon-coupled systems. In this scheme, we calculate partially renormalized phonon frequencies and electron-phonon coupling, which include the screening effects of high-energy electrons, to construct a realistic Hamiltonian consisting of low-energy electron and phonon degrees of freedom. We show that our scheme can be implemented by slightly modifying the density functional-perturbation theory (DFPT), which is one of the standard methods for calculating phonon properties from first principles. Our scheme, which we call the constrained DFPT, can be applied to various phonon-related problems, such as superconductivity, electron and thermal transport, thermoelectricity, piezoelectricity, dielectricity, and multiferroicity. We believe that the constrained DFPT provides a firm basis for the understanding of the role of phonons in strongly correlated materials. Here, we apply the scheme to fullerene superconductors and discuss how the realistic low-energy Hamiltonian is constructed.

DOI: 10.1103/PhysRevB.92.245108 PACS number(s): 63.20.dk, 71.27.+a, 74.25.Kc

I. INTRODUCTION

A quantitative description of strongly correlated materials is one of the most challenging goals in condensed matter physics. In particular, an accurate treatment of the lattice degrees of freedom in the strongly correlated regime is necessary for a description or even a prediction of functional materials such as high-transition-temperature (high-T_c) superconductors, thermoelectrics, piezoelectrics, and multiferroics. However, the interplay between strong correlation and electron-phonon coupling has yet to be fully understood. For example, the role of the electron-phonon interaction in cuprate superconductors is still controversial [1–5]. Recently, it has been proposed that the electron correlation enhances electron-phonon coupling [6–9]. The phonon might cooperate with plasmons to realize high-T_c superconductivity [10–12]. It has been shown that an unusual cooperation between the multiorbital electronic correlation and Jahn-Teller phonons is the essence of high-T_c s-wave superconductivity next to the Mott insulating phase in fullerides [13–16].

In this paper, we propose that a combination of the density-functional theory (DFT) and model calculations, which is one of the most powerful methods to study the strongly correlated materials [17–19], can also be powerful in studying electron-phonon-coupled systems with strong electron correlations. This idea relies on the energy hierarchy in the electronic structure [19]: By the strong electronic correlation and the electron-phonon coupling, the low-energy bands near the Fermi level E_F, which we call target bands, may be heavily reconstructed, while the structure of the high-energy bands will not change drastically. Furthermore, at a temperature where the low-energy phenomena (e.g., superconductivity) emerge, the high-energy states are nearly frozen, i.e., they are nearly totally occupied or empty. Then, nearly all the excitation processes occur in the t subspace, the subspace which the target bands span (for later use, we define the r subspace as the rest of the Hilbert space). The most important electron-phonon coupling processes are the couplings between these t-subspace electrons and phonons. Therefore, the low-energy physical properties are governed by the low-energy electrons and the phonons.

This hierarchical structure allows us to construct the following three-stage scheme [19].

(1) Obtain the global energy structure by the DFT and define the low-energy subspace.

(2) Trace out the high-energy electron degrees of freedom and derive a low-energy effective Hamiltonian (downfolding). The degrees of freedom in the Hamiltonian consist of the t-subspace electrons and the phonons.

(3) Solve the derived model accurately by the model-calculation method.

In this scheme, we take into account the material dependence and the high-energy electronic structure by the DFT, and the effects of electron correlation and electron-phonon coupling in the low-energy subspace (t subspace) are considered by the model calculation. A key step in the scheme is step 2, i.e., the downfolding procedure to derive the low-energy Hamiltonian.

When we restrict ourselves to the electron degrees of freedom and forget about the phonons, there has been much effort devoted to the development of a downfolding scheme. In this case, the low-energy Hamiltonian would consist of the electron one-body (hopping) and Coulomb interaction terms. By employing a localized basis such as the maximally localized Wannier function [20–22], the derived model has the form of the extended Hubbard model. The one-body part describes a realistic hopping structure in the t subspace. The effective interaction between t-subspace electrons is a partially screened Coulomb interaction. This is because the high-energy electrons, which are traced out, cause a renormalization of the Coulomb interaction. We refer to it as a "partially" screened interaction because it does not include screening

*Present address: Centre de Physique Théorique, École Polytechnique, CNRS, Université Paris-Saclay, F-91128 Palaiseau, France; yusuke.nomura@riken.jp

processes originating from t-subspace electrons, which are *not* traced out and remain as active degrees of freedom. This partial screening is often calculated within the constrained random phase approximation (cRPA) [23], which considers the screening effect of high-energy electrons within the RPA.

The downfolding scheme combined with the model-calculation method has been successfully applied to, e.g., iron-based superconductors [24–29], cuprates [30–33], transition-metal oxides [34,35], and organic compounds [36,37]. Based on these successes, many attempts have been made to further improve the scheme. For example, there have been proposals to improve the one-body part [38,39] and the interaction part [40–45]. Recently, a GW-based (not DFT-based) scheme has also been intensively studied [46–49].

Despite the effort devoted to electronic systems, an *ab initio* downfolding scheme for electron-phonon coupled systems has not been established. If we include the phonon degrees of freedom, the low-energy model acquires the electron-phonon coupling and phonon one-body terms in addition to the electron one-body and Coulomb interaction terms. As in the case of effective Coulomb interaction between t-subspace electrons, the electron-phonon coupling and phonon frequencies used in the low-energy Hamiltonian should be a partially renormalized quantity [50]. They are renormalized due to the coupling between phonons and high-energy electrons. The coupling between phonons and t-subspace electrons is considered when we solve the model by the model-calculation method. When we derive the model, the renormalization originating from the t subspace is excluded to avoid the double-counting of it. Based on this idea, we recently proposed an *ab initio* scheme called the constrained density-functional perturbation theory (cDFPT) [51].

In this paper, we elaborate the practical detail of the cDFPT method. We show that the cDFPT method can be easily implemented by a slight modification of the conventional DFPT method, which is implemented in several *ab initio* packages. Then we apply the scheme to alkali-doped fullerides [52–54], where both electron correlations and electron-phonon interactions are important to explain the phase diagram [13]. By comparing the cDFPT results with the DFPT results, we discuss how the partially screened quantities, which are used as input for the model calculation, differ from the fully renormalized quantities.

This paper is organized as follows. In Sec. II, we review the DFPT [55–58] to introduce our notation, since the cDFPT method is closely related to the conventional DFPT. Then we move on to the explanation of the cDFPT method in Sec. III. There, we provide practical details to implement the cDFPT method. We also briefly compare the cDFPT method and another downfolding method proposed in Ref. [59]. In Sec. IV, we show the cDFPT results for alkali-doped fullerides and compare them with the DFPT results. Finally, in Sec. V, we provide a summary of the paper.

II. REVIEW OF DENSITY-FUNCTIONAL PERTURBATION THEORY

The cDFPT method is based on the DFPT method, where the fully renormalized electron-phonon coupling and phonon frequencies are calculated. As we show below, the cDFPT method can be formulated as a slight modification of the DFPT algorithm. Here, we briefly review the DFPT method [55–58] to introduce the notation used here.

A. Phonon frequencies

1. Expression for interatomic force constants

In solids, phonon frequencies are determined by the equation [58]

$$\sum_{\kappa'\alpha'} D^{\alpha\alpha'}_{\kappa\kappa'}(\mathbf{q}) e^{\alpha'}_{\kappa'}(\mathbf{q}) = \omega^2_{\mathbf{q}\nu} e^{\alpha}_{\kappa}(\mathbf{q}\nu), \tag{1}$$

with momentum $\mathbf{q}$, index for atoms κ, and direction of displacement $\alpha = \{x,y,z\}$. This equation shows that the phonon frequency $\omega_{\mathbf{q}\nu}$ is given by the square root of the eigenvalues of the dynamical matrix $D(\mathbf{q})$. Since the dimension of the dynamical matrix $D(\mathbf{q})$ is $3n$, with n being the number of atoms in the unit cell, there exist $3n$ solutions (normal modes), which we label with the index ν. The eigenvectors of the dynamical matrix satisfy the orthonormality:

$$\sum_{\kappa\alpha} e^{*\alpha}_{\kappa}(\mathbf{q}\nu) e^{\alpha}_{\kappa}(\mathbf{q}\nu') = \delta_{\nu\nu'}. \tag{2}$$

The dynamical matrix is related to the interatomic force constants $C^{\alpha\alpha'}_{\kappa\kappa'}(\mathbf{q})$ by

$$D^{\alpha\alpha'}_{\kappa\kappa'}(\mathbf{q}) = \frac{1}{\sqrt{M_\kappa M_{\kappa'}}} C^{\alpha\alpha'}_{\kappa\kappa'}(\mathbf{q}), \tag{3}$$

where M_κ is the mass of the κth atom. The interatomic force constants are written as [58]

$$\begin{aligned} C^{\alpha\alpha'}_{\kappa\kappa'}(\mathbf{q}) = \frac{1}{N}\Bigg[& \int \left(\frac{\partial \rho(\mathbf{r})}{\partial u^{\alpha}_{\kappa}(\mathbf{q})} \right)^{*} \frac{\partial V_{\mathrm{ion}}(\mathbf{r})}{\partial u^{\alpha'}_{\kappa'}(\mathbf{q})} d\mathbf{r} \\ & + \int \rho(\mathbf{r}) \frac{\partial^2 V_{\mathrm{ion}}(\mathbf{r})}{\partial u^{*\alpha}_{\kappa}(\mathbf{q}) \partial u^{\alpha'}_{\kappa'}(\mathbf{q})} d\mathbf{r} \\ & + \frac{\partial^2 E_N}{\partial u^{*\alpha}_{\kappa}(\mathbf{q}) \partial u^{\alpha'}_{\kappa'}(\mathbf{q})} \Bigg]_{u=0}, \end{aligned} \tag{4}$$

with the number of unit cells in the Born–von Karman boundary condition N, the displacement of the ion u, the electron density ρ, the ionic potential V_{ion}, and the Coulomb interaction energy among nuclei E_N. On the right-hand side (r.h.s.) of Eq. (4), the first (second) term describes the contribution from linear (quadratic) electron-phonon coupling and the third term describes the ionic contribution [60].

2. Electron-density response

In order to evaluate the interatomic force constants, we need to calculate the electron-density response to the ionic displacement $\partial\rho(\mathbf{r})/\partial u^{\alpha}_{\kappa}(\mathbf{q})$, which is a key quantity in the cDFPT method, as we show below. Before explaining the cDFPT, we show how the electron-density response is calculated in the usual DFPT method. Here, we consider a metallic case [56]. In the DFT calculation for a metal, it is usual to introduce a smearing function, $\tilde{\delta}(x)$, and the corresponding smoothed step function $\tilde{\theta}(x) = \int_{-\infty}^{x} \tilde{\delta}(x')dx'$. In the present calculation, we employ the Gaussian smearing $\tilde{\delta}(x) = \exp(-x^2)/\sqrt{\pi}$. Then

the expression for the electron-density response $\Delta\rho(\mathbf{r})$ to ionic displacement is given by

$$\begin{aligned}\Delta\rho(\mathbf{r}) &= \sum_{n,m} \frac{\tilde{\theta}_{F,n} - \tilde{\theta}_{F,m}}{\varepsilon_n - \varepsilon_m} \psi_n^*(\mathbf{r})\psi_m(\mathbf{r})\langle\psi_m|\Delta V_{\rm SCF}|\psi_n\rangle \\ &= 2\sum_n \psi_n^*(\mathbf{r})\Delta\psi_n(\mathbf{r}), \end{aligned} \tag{5}$$

where we define $\Delta\psi_n(\mathbf{r})$ as

$$\Delta\psi_n(\mathbf{r}) = \sum_m \frac{\tilde{\theta}_{F,n} - \tilde{\theta}_{F,m}}{\varepsilon_n - \varepsilon_m} \tilde{\theta}_{m,n}\psi_m(\mathbf{r})\langle\psi_m|\Delta V_{\rm SCF}|\psi_n\rangle, \tag{6}$$

with composite indices for the band and the momentum n,m, the Kohn-Sham wave function ψ_n, and the Kohn-Sham eigenenergy ε_n. Here, $\tilde{\theta}_{F,n}$ and $\tilde{\theta}_{m,n}$ are defined as $\tilde{\theta}_{F,n} = \tilde{\theta}[(\varepsilon_F - \varepsilon_n)/\sigma]$ and $\tilde{\theta}_{m,n} = \tilde{\theta}[(\varepsilon_m - \varepsilon_n)/\sigma]$, respectively, with the Fermi energy ε_F and a smearing width σ. In the actual calculation, the electron-density response $\Delta\rho$ and the modulation of the potential $\Delta V_{\rm SCF}$ have indices of the momentum $\mathbf{q}$, the displaced atom κ, and the direction α, which we omit for simplicity. The change in the potential $\Delta V_{\rm SCF}$ due to ionic displacement is given by a sum of the change in the ionic potential $\Delta V_{\rm ion}$ and the screening contribution from the Hartree and exchange channels (the second and third terms on the r.h.s. of the following equation),

$$\begin{aligned}\Delta V_{\rm SCF}(\mathbf{r}) = \Delta V_{\rm ion}(\mathbf{r}) &+ e^2 \int \frac{\Delta\rho(\mathbf{r}')}{|\mathbf{r} - \mathbf{r}'|} d\mathbf{r}' \\ &+ \left.\frac{dV_{\rm xc}[\rho]}{d\rho}\right|_{\rho=\rho_0(\mathbf{r})} \Delta\rho(\mathbf{r}), \end{aligned} \tag{7}$$

with ρ_0 being the electron density in the absence of ionic displacement. Equations (5) and (7) are the equations to determine the electron-density response, which are solved self-consistently.

In the DFPT, in order to avoid the cumbersome summation over unoccupied states in Eq. (6), one alternatively solves the equations (Eqs. (72) and (73) in Ref. [58])

$$(\mathcal{H}_{\rm SCF} + Q - \varepsilon_n)|\Delta\psi_n\rangle = -(\tilde{\theta}_{F,n} - P_n)\Delta V_{\rm SCF}|\psi_n\rangle, \tag{8}$$

where

$$Q = \sum_m \alpha_m |\psi_m\rangle\langle\psi_m|, \quad P_n = \sum_m \beta_{n,m}|\psi_m\rangle\langle\psi_m|, \tag{9}$$

with

$$\beta_{n,m} = \tilde{\theta}_{F,n}\tilde{\theta}_{n,m} + \tilde{\theta}_{F,m}\tilde{\theta}_{m,n} + \alpha_m \frac{\tilde{\theta}_{F,n} - \tilde{\theta}_{F,m}}{\varepsilon_n - \epsilon_m}\tilde{\theta}_{m,n}. \tag{10}$$

Here α_m's are parameters to avoid null eigenvalues of the $(\mathcal{H}_{\rm SCF} + Q - \varepsilon_n)$ matrix, which can be set to be a constant value which is larger than [(maximum energy among partial occupied states) − (minimum energy of occupied states)] for all partially occupied states and 0 for totally unoccupied states [58]. This α_m parametrization enables the calculation without any information on the totally unoccupied states. In Appendix A, we show that the solution of Eq. (8) is indeed identical to that of Eq. (6).

When the perturbation has periodicity with the lattice ($\mathbf{q} = \mathbf{0}$), the Fermi energy may change and $\Delta\rho$ acquires an additional term [58],

$$\Delta\rho(\mathbf{r}) = 2\sum_n \psi_n^*(\mathbf{r})\Delta\psi_n(\mathbf{r}) + \rho(\mathbf{r},\varepsilon_F)\Delta\varepsilon_F, \tag{11}$$

with

$$\rho(\mathbf{r},\varepsilon) = \sum_n \frac{1}{\sigma}\tilde{\delta}\left(\frac{\varepsilon - \varepsilon_n}{\sigma}\right)|\psi_n(\mathbf{r})|^2. \tag{12}$$

The change in the Fermi energy $\Delta\varepsilon_F$ is determined by the charge neutrality condition [58].

B. Electron-phonon coupling

When ions move from their equilibrium position, the ionic potential changes. Then the surrounding electrons will respond to the potential change and screen it. The electron will feel this screened potential change and will be scattered. This process is expressed by the Hamiltonian

$$\hat{\mathcal{H}}_{\text{el-ph}} = \frac{1}{\sqrt{N}} \sum_{\mathbf{q}\nu} \sum_{\mathbf{k}nn'\sigma} g^{\nu}_{n'n}(\mathbf{k},\mathbf{q}) c^{\sigma\dagger}_{n'\mathbf{k}+\mathbf{q}} c^{\sigma}_{n\mathbf{k}} (b_{\mathbf{q}\nu} + b^{\dagger}_{-\mathbf{q}\nu}). \tag{13}$$

Here,

$$\begin{aligned} g^{\nu}_{n'n}(\mathbf{k},\mathbf{q}) = &\sum_{\kappa\alpha} \sqrt{\frac{\hbar}{2M_\kappa\omega_{\mathbf{q}\nu}}}\, e^{\alpha}_{\kappa}(\mathbf{q}\nu) \\ &\times \left\langle \psi_{n'\mathbf{k}+\mathbf{q}} \left| \frac{\partial V_{\rm SCF}(\mathbf{r})}{\partial u^{\alpha}_{\kappa}(\mathbf{q})} \right| \psi_{n\mathbf{k}} \right\rangle \end{aligned} \tag{14}$$

is the electron-phonon-coupling matrix element involving the Bloch states $\psi_{n\mathbf{k}}$ and $\psi_{n'\mathbf{k}+\mathbf{q}}$ and the νth branch phonon with wave vector $\mathbf{q}$. $c^{\sigma}_{n\mathbf{k}}$ ($c^{\sigma\dagger}_{n\mathbf{k}}$) annihilates (creates) an electron on the nth Bloch orbital with wave vector $\mathbf{k}$ and spin σ. $b_{\mathbf{q}\nu}$ ($b^{\dagger}_{\mathbf{q}\nu}$) is the annihilation (creation) operator for the phonon labeled by the νth branch and the momentum $\mathbf{q}$.

III. CONSTRAINED DENSITY-FUNCTIONAL PERTURBATION THEORY

A. Basic idea and practical implementation

Our goal is to derive the low-energy Hamiltonian for electron-phonon-coupled systems, which consists of low-energy (t-subspace) electrons and phonons. The Hamiltonian reads

$$\hat{\mathcal{H}} = \hat{\mathcal{H}}_{\text{el}} + \hat{\mathcal{H}}_{\text{el-el}} + \hat{\mathcal{H}}_{\text{el-ph}} + \hat{\mathcal{H}}_{\text{ph}} + \hat{\mathcal{H}}_{\text{DC}}, \tag{15}$$

where $\hat{\mathcal{H}}_{\text{el}}$ is the electronic one-body part (on-site energy and hopping terms) and $\hat{\mathcal{H}}_{\text{el-el}}$ is the Coulomb interaction term, such as the Hubbard U. In this paper, we focus on the electron-phonon coupling $\hat{\mathcal{H}}_{\text{el-ph}}$ and phonon one-body term $\hat{\mathcal{H}}_{\text{ph}}$, which are given by

$$\hat{\mathcal{H}}_{\text{el-ph}} = \frac{1}{\sqrt{N}} \sum_{\mathbf{q}\nu} \sum_{\mathbf{k}ij\sigma} g^{(p)\nu}_{ij}(\mathbf{k},\mathbf{q}) c^{\sigma\dagger}_{i\mathbf{k}+\mathbf{q}} c^{\sigma}_{j\mathbf{k}} (b_{\mathbf{q}\nu} + b^{\dagger}_{-\mathbf{q}\nu}) \tag{16}$$

and

$$\hat{\mathcal{H}}_{\rm ph} = \sum_{\mathbf{q}\nu} \omega^{(p)}_{\mathbf{q}\nu} b^\dagger_{\mathbf{q}\nu} b_{\mathbf{q}\nu}, \tag{17}$$

respectively. Here, we employ the Wannier gauge for the electronic degrees of freedom labeled i,j, since it is convenient for low-energy solvers to take the Wannier gauge. $\hat{\mathcal{H}}_{\rm DC}$ is a double-counting correction, which is discussed in detail in Sec. III D. In this section, we show how the phonon frequencies $\omega^{(p)}$ and the electron-phonon coupling $g^{(p)}$ in the low-energy model should be parametrized [51]. As in the case of the effective Coulomb interactions in $\hat{\mathcal{H}}_{\text{el-el}}$ calculated by the cRPA method [23], they should be partially renormalized quantities, which take into account the renormalization effects associated with the elimination of high-energy degrees of freedom (see Appendix B for a comparison between the cDFPT and the cRPA). In other words, we derive the parameters while avoiding double-counting of the renormalization effects, which are to be taken into account in the model analysis step. To make it clear that these are partially renormalized quantities, we attach the superscript (p).

In the following, we discuss how the partially renormalized phonon quantities are calculated from first principles. For partial renormalization, we first define the bare phonon frequencies and electron-phonon coupling. We then divide the renormalization processes into the low-energy contribution, which is to be excluded to realize partial renormalization, and the rest of the contribution, which involves high-energy electrons.

First, we consider the phonon frequencies. As we see in Sec. II A, the interatomic force constants [Eq. (4)], which give the phonon frequencies, consist of several contributions. Since the low-energy Hamiltonian, Eq. (15), has the linear electron-phonon coupling term, which gives a renormalization of the phonon frequencies, we define (ionic contribution) + (contribution from quadratic electron-phonon coupling) as the "bare" term and (contribution from linear electron-phonon coupling) as the "renormalizing" term. Then the interatomic force constants $C^{\alpha\alpha'}_{\kappa\kappa'}(\mathbf{q})$ given in Eq. (4) can be divided as $C^{\alpha\alpha'}_{\kappa\kappa'}(\mathbf{q}) = {}^{\rm bare}C^{\alpha\alpha'}_{\kappa\kappa'}(\mathbf{q}) + {}^{\rm ren.}C^{\alpha\alpha'}_{\kappa\kappa'}(\mathbf{q})$, where ${}^{\rm bare}C^{\alpha\alpha'}_{\kappa\kappa'}(\mathbf{q})$ gives the bare phonon frequencies,

$${}^{\rm bare}C^{\alpha\alpha'}_{\kappa\kappa'}(\mathbf{q}) = \frac{1}{N}\left[\frac{\partial^2 E_{\rm N}}{\partial u^{*\alpha}_\kappa(\mathbf{q})\partial u^{\alpha'}_{\kappa'}(\mathbf{q})} + \int \rho(\mathbf{r})\frac{\partial^2 V_{\rm ion}(\mathbf{r})}{\partial u^{*\alpha}_\kappa(\mathbf{q})\partial u^{\alpha'}_{\kappa'}(\mathbf{q})}d\mathbf{r}\right], \tag{18}$$

and ${}^{\rm ren.}C^{\alpha\alpha'}_{\kappa\kappa'}(\mathbf{q})$ gives the renormalization of the phonon frequencies through the linear electron-phonon coupling,

$${}^{\rm ren.}C^{\alpha\alpha'}_{\kappa\kappa'}(\mathbf{q}) = \frac{1}{N}\int\left(\frac{\partial\rho(\mathbf{r})}{\partial u^\alpha_\kappa(\mathbf{q})}\right)^* \frac{\partial V_{\rm ion}(\mathbf{r})}{\partial u^{\alpha'}_{\kappa'}(\mathbf{q})}d\mathbf{r}. \tag{19}$$

Next, we consider the bare and renormalizing contributions to electron-phonon coupling [Eq. (14)]. The derivative of the self-consistent field potential $\partial V_{\rm SCF}(\mathbf{r})/\partial u^\alpha_\kappa(\mathbf{q})$ in Eq. (14) is also decomposed into the bare contribution,

$${}^{\rm bare}\left[\frac{\partial V_{\rm SCF}(\mathbf{r})}{\partial u^\alpha_\kappa(\mathbf{q})}\right] = \frac{\partial V_{\rm ion}(\mathbf{r})}{\partial u^\alpha_\kappa(\mathbf{q})}, \tag{20}$$

and the screening contribution (the change in the Hartree and exchange potentials),

$${}^{\rm ren.}\left[\frac{\partial V_{\rm SCF}(\mathbf{r})}{\partial u^\alpha_\kappa(\mathbf{q})}\right] = \int\left(\frac{e^2}{|\mathbf{r}-\mathbf{r}'|} + \frac{dV_{\rm xc}(\mathbf{r})}{d\rho}\delta(\mathbf{r}-\mathbf{r}')\right) \times \frac{\partial\rho(\mathbf{r}')}{\partial u^\alpha_\kappa(\mathbf{q})}d\mathbf{r}'. \tag{21}$$

We see that the origin of the renormalization of the phonon frequencies and the screening for electron-phonon couplings is the coupling between the lattice and the electrons and the resulting modulation of the electron density due to the lattice displacement $\partial\rho(\mathbf{r})/\partial u^\alpha_\kappa(\mathbf{q})$. The electron-density modulation $\partial\rho(\mathbf{r})/\partial u^\alpha_\kappa(\mathbf{q})$ calculated in the conventional DFPT scheme is a sum of the contributions from all possible particle-hole excitations [Eq. (5)]. In the cDFPT method [51], we exclude the target $\leftrightarrow$ target excitation processes from the sum in the calculation of the electron-density modulation. We use the resulting electron-density modulation for the renormalization contributions in Eqs. (19) and (21), which are added to the bare contributions in Eqs. (18) and (20). This procedure gives the partially renormalized phonon frequencies and the electron-phonon couplings.

Now, we propose a practical way to exclude the target $\leftrightarrow$ target processes from Eqs. (5) and (8), the equations which determine the change in the electron density. If $|\psi_n\rangle$ in Eq. (8) belongs to the t subspace, in order to exclude the target $\leftrightarrow$ target polarization processes, the r.h.s. of Eq. (8) should be modified as

$$(\mathcal{H}_{\rm SCF} + Q - \varepsilon_n)|\Delta\psi_n\rangle = -P_r(\tilde{\theta}_{F,n} - P_n)\Delta V_{\rm SCF}|\psi_n\rangle, \tag{22}$$

with P_r being the projection onto the r subspace. The very same constraint can be achieved by solving Eq. (8) with modified $\beta_{n,m}$'s ($\tilde{\beta}_{n,m}$'s) given by

$$\tilde{\beta}_{n,m} = \begin{cases} \tilde{\theta}_{F,n} & (n,m \in t\text{-subspace}), \\ \tilde{\theta}_{F,n}\tilde{\theta}_{n,m} + \tilde{\theta}_{F,m}\tilde{\theta}_{m,n} + \alpha_m\frac{\tilde{\theta}_{F,n}-\tilde{\theta}_{F,m}}{\varepsilon_n-\varepsilon_m}\tilde{\theta}_{m,n} & (\text{other cases}). \end{cases} \tag{23}$$

Note that in the latter case, $\tilde{\beta}_{n,m}$ has exactly the same form as that in Eq. (10), i.e., $\tilde{\beta}_{n,m} = \beta_{n,m}$. Only when $n,m \in t$ subspace, $\beta_{n,m}$ is modified. We can easily show that the r.h.s. of Eq. (22) with the original $\beta_{n,m}$'s is equal to that of Eq. (8) with $\tilde{\beta}_{n,m}$'s, which ensures the equivalence of the two types of modifications. Using $\tilde{\beta}_{n,m}$ in Eq. (23) is also useful to exclude the contribution to the electron-density modulation from the possible change in the Fermi energy in the case of $\mathbf{q} = \mathbf{0}$ [the additional contribution given in Eqs. (11) and (12)]. The possible change in Fermi energy originates from intraband transitions at the Fermi level, which are the transition processes in the t subspace and hence are excluded by employing $\tilde{\beta}_{n,m}$.

When we consider practical implementation, if one has a code of the conventional DFPT, it is easier to modify $\beta_{n,m}$ into $\tilde{\beta}_{n,m}$ than to employ Eq. (22). One needs only to modify the part where the $\beta_{n,m}$ parameters are defined; no modification is needed in the other parts. In Appendix C, we propose an example of how we modify a source code to introduce $\tilde{\beta}_{n,m}$ in the case of the QUANTUM ESPRESSO

package [61,62]. With $\tilde{\beta}_{n,m}$'s and following the very same flow of calculations as in the usual DFPT method, one can calculate the electron-density response to ionic displacement without target $\leftrightarrow$ target polarization processes. Then, with the resulting electron-density response, we evaluate the partially renormalized quantities $\omega^{(p)}$ and $g^{(p)}$.

B. Relation between fully and partially renormalized quantities

In this section, we show the relation between partially and fully renormalized quantities. Partially (fully) renormalized quantities are calculated by the cDFPT (conventional DFPT) method. The electron-density response $\Delta\rho$ to the change in the ionic potential $\Delta V_{\rm ion}$ (bare perturbation) is given by [63]

$$\Delta\rho = \underbrace{\chi^0(1-\tilde{v}\chi^0)^{-1}}_{=\chi_{\rm DFT}}\Delta V_{\rm ion} \tag{24}$$

$$= \chi^0 \Delta V_{\rm SCF}, \tag{25}$$

where $\Delta V_{\rm SCF}$ is the screened potential change, given by

$$\Delta V_{\rm SCF} = (1-\tilde{v}\chi^0)^{-1}\Delta V_{\rm ion}. \tag{26}$$

Here, $\tilde{v}$ is given by $\tilde{v} = v + K_{\rm xc}$, with the bare Coulomb interaction v and the exchange-correlation kernel $K_{\rm xc} = \delta V_{\rm xc}/\delta\rho$ ($V_{\rm xc}$ is the exchange-correlation potential). Note that Eqs. (25) and (26) correspond to Eqs. (5) and (7), respectively. The screening expressed in Eq. (26) can be divided into two screening steps: one involving the high-energy degrees of freedom,

$$\Delta V^{(p)}_{\rm SCF} = \left(1-\tilde{v}\chi^0_r\right)^{-1}\Delta V_{\rm ion}, \tag{27}$$

and the other associated with the target-target processes,

$$\Delta V^{(f)}_{\rm SCF} = \left(1-\tilde{W}^{(p)}\chi^0_t\right)^{-1}\Delta V^{(p)}_{\rm SCF}. \tag{28}$$

Here, the total irreducible polarization χ^0 is divided into χ^0_t and χ^0_r with the polarization within the t subspace χ^0_t and the rest of the polarization $\chi^0_r = \chi^0 - \chi^0_t$. We have introduced the superscripts p and f to explicitly distinguish between partially (p) and fully (f) renormalized quantities. $\tilde{W}^{(p)}$ is the partially screened Coulomb interaction given by

$$\tilde{W}^{(p)} = \left(1-\tilde{v}\chi^0_r\right)^{-1}\tilde{v}. \tag{29}$$

Since the electron-phonon coupling g represents the scattering of electrons by $\Delta V_{\rm SCF}$, the screening process for electron-phonon coupling can be decomposed in the very same way as that of $\Delta V_{\rm SCF}$ [Eqs. (27) and (28)]; that is, $g^{(f)} = (1-\tilde{v}\chi^0)^{-1}g^{(b)}$ is decomposed into

$$g^{(p)} = \left(1-\tilde{v}\chi^0_r\right)^{-1}g^{(b)} \tag{30}$$

and

$$g^{(f)} = \left(1-\tilde{W}^{(p)}\chi^0_t\right)^{-1}g^{(p)}. \tag{31}$$

Equation (31) tells us that when we take into account target-target screening processes at the DFT level for the model with partially screened Coulomb and electron-phonon interactions, we return to the fully screened electron-phonon interactions.

A similar decomposition also applies to the renormalization of the phonon frequencies. In this case, the phonon self-energy is decomposed. The renormalizing contribution to the interatomic force constants in Eq. (19) can be recast as

$${}^{\rm ren.}C = |g'^{(b)}|^2\chi_{\rm DFT}, \tag{32}$$

where $g'^{(b)} = \sqrt{2M\omega^{(b)}}g^{(b)}$, with $\omega^{(b)}$ being the bare phonon frequency. For simplicity, we have omitted the indices and represent the masses of the nucleus by a single mass M. We define the phonon self-energy in the DFPT scheme as

$$\Sigma = \frac{{}^{\rm ren.}C}{2M\omega^{(b)}} = |g^{(b)}|^2\chi_{\rm DFT}. \tag{33}$$

The contribution to the phonon self-energy can be divided into Σ_t and Σ_r, i.e.,

$$\Sigma = \Sigma_t + \Sigma_r. \tag{34}$$

Here, $\Sigma_r = |g^{(b)}|^2\chi^r_{\rm DFT}$, with $\chi^r_{\rm DFT} = \chi^0_r(1-\tilde{v}\chi^0_r)^{-1}$, denotes the phonon self-energy due to electron-phonon coupling involving r-subspace electrons. The other part of the self-energy, $\Sigma_t = |g^{(p)}|^2\chi^t_{\rm DFT}$, with $\chi^t_{\rm DFT} = \chi^0_t(1-\tilde{W}^{(p)}\chi^0_t)^{-1}$, originates from the coupling between t subspace electrons and phonons through the partially screened coupling $g^{(p)}$. See Appendix D for the proof that $\Sigma_t + \Sigma_r = |g^{(p)}|^2\chi^t_{\rm DFT} + |g^{(b)}|^2\chi^r_{\rm DFT}$ is indeed identical to $\Sigma = |g^{(b)}|^2\chi_{\rm DFT}$. The decomposition of Σ into Σ_t and Σ_r corresponds to the division of the density-response contribution to ${}^{\rm ren.}C$ into the target-target contribution and the others, as in the cDFPT scheme. With the decomposition of Σ, we can define the partially dressed phonon Green's function $D^{(p)}$ as

$$[D^{(p)}]^{-1} = [D^{(b)}]^{-1} - \Sigma_r, \tag{35}$$

with the bare phonon Green's function $D^{(b)}$. The bare phonon frequency $\omega^{(b)}$ is given by the pole of $D^{(b)}$. Similarly, the phonon frequency $\omega^{(p)}$ in the low-energy Hamiltonian is given by the pole of $D^{(p)}$. If we further consider Σ_t, we obtain the fully dressed phonon Green's function $D^{(f)}$ as

$$[D^{(f)}]^{-1} = [D^{(p)}]^{-1} - \Sigma_t. \tag{36}$$

C. Flow of the calculation and practical issues

As already mentioned, the flow of the cDFPT calculation follows that of the usual DFPT. The difference comes from the setting of the $\beta_{n,m}$ parameters. The flow of the calculation is as follows:

(1) Optimize the atomic positions within the DFT.

(2) Calculate the global energy structure by the DFT for the optimized structure and choose the target subspace for which we construct an effective Hamiltonian.

(3) Set the $\tilde{\beta}_{n,m}$ parameters according to Eq. (23).

(4) Perform the phonon calculation with the $\tilde{\beta}_{n,m}$ parameters (the procedure is the very same as in the conventional DFPT case). Obtain the partially renormalized phonon frequencies $\omega^{(p)}_{\mathbf{q}\nu}$ to be used in Eq. (17) and the partially screened potential change $\frac{\partial V^{(p)}_{\rm SCF}(\mathbf{r})}{\partial u^\alpha_\kappa(\mathbf{q})}$.

(5) Take the Wannier matrix element of $\frac{\partial V^{(p)}_{\rm SCF}(\mathbf{r})}{\partial u^\alpha_\kappa(\mathbf{q})}$ to obtain the partially renormalized electron-phonon coupling term in

Eq. (16) as follows:

$$g_{ij}^{(p)\nu}(\mathbf{k},\mathbf{q}) = \sum_{\kappa\alpha}\sqrt{\frac{\hbar}{2M_\kappa\omega_{\mathbf{q}\nu}^{(p)}}}\,e_\kappa^{(p)\alpha}(\mathbf{q}\nu) \times\left\langle\psi_{i\mathbf{k}+\mathbf{q}}^{(w)}\left|\frac{\partial V_{\mathrm{SCF}}^{(p)}(\mathbf{r})}{\partial u_\kappa^\alpha(\mathbf{q})}\right|\psi_{j\mathbf{k}}^{(w)}\right\rangle, \tag{37}$$

where we use the superscript (w) to make it clear that the wave function is in the Wannier gauge.

Finally, we mention one practical issue in obtaining the partially screened phonon frequencies $\omega_{\mathbf{q}\nu}^{(p)}$. In obtaining the fully renormalized phonon frequencies, we often impose the acoustic sum rule to ensure that the frequency of the acoustic phonon at $\mathbf{q}=\mathbf{0}$ is 0. To obtain the partially renormalized phonon frequencies, we impose the same correction of the acoustic sum rule as used in the calculation of the fully renormalized phonon frequencies. Then the partially renormalized phonon frequency of the acoustic phonon at $\mathbf{q}=\mathbf{0}$ does not always go to 0. This is because the phonon self-energy involving t-subspace electrons $\Sigma_t = |g^{(p)}|^2\chi_{\mathrm{DFT}}^t$ can be finite, since there can be a finite coupling between the acoustic phonon and t-subspace electrons through Umklapp ($\mathbf{G}\neq\mathbf{0}$) processes, while the coupling for the $\mathbf{q}+\mathbf{G}=\mathbf{0}$ process is 0. We also give another explanation for possible nonzero phonon frequency for the acoustic mode at $\mathbf{q}=\mathbf{0}$. For example, in the case where the unit cell consists of a single atom, at $\mathbf{q}=\mathbf{0}$, the ionic contribution to the interatomic force constant [the third term on the r.h.s. of Eq. (4)] is 0. The first (second) term on the r.h.s. of Eq. (4), which is related to the linear (quadratic) electron-phonon coupling, makes a negative (positive) contribution to the interatomic force constant. Since the first and second terms cancel each other, the fully renormalized phonon frequency at $\mathbf{q}=\mathbf{0}$ goes to 0. In the cDFPT, we exclude the target contribution to the first term, thus imbalance occurs between the first and the second terms, which makes the partially renormalized phonon frequency nonzero.

D. Double-counting correction

When we combine the DFT and the model-calculation methods, we usually need a double-counting correction. In the case of our scheme, we have a double-counting problem for a possible change in equilibrium positions of the atoms due to the coupling between lattice and t-subspace electrons. The low-energy Hamiltonian should be formulated such that we obtain equilibrium positions of the ions which agree with the optimized positions within the DFT level, after we solve the model at the static mean-field (DFT) level. To realize this, we need a double-counting correction in the low-energy Hamiltonian, whose form is

$$\hat{\mathcal{H}}_{\mathrm{DC}} = -\frac{1}{\sqrt{N}}\sum_{\nu}\sum_{\mathbf{k}ij\sigma} g_{ij}^{(p)\nu}(\mathbf{k},\mathbf{q}=\mathbf{0})\langle c_{i\mathbf{k}}^{\sigma\dagger}c_{j\mathbf{k}}^{\sigma}\rangle\left(b_{\mathbf{0}\nu}+b_{\mathbf{0}\nu}^\dagger\right). \tag{38}$$

Here, $\langle c_{i\mathbf{k}}^{\sigma\dagger}c_{j\mathbf{k}}^{\sigma}\rangle$ is the expectation value evaluated within the DFT.

To understand the physical meaning of the double-counting correction, we consider a simple case, where the t subspace consists of a single band and only one Holstein phonon couples to the electron locally. Then the electron-phonon coupling term in Eq. (16) is given by

$$\hat{\mathcal{H}}_{\text{el-ph}} = \sum_l g^{(p)} n_l x_l, \tag{39}$$

where we switch to the real-space representation and l is the site index. n_l is the density operator for site l and x_l is the displacement of the lattice. The double-counting correction [Eq. (38)] becomes

$$\hat{\mathcal{H}}_{\mathrm{DC}} = -\sum_l g^{(p)}\langle n_l\rangle x_l. \tag{40}$$

If we put together the electron-phonon coupling, double-counting, and potential energy terms [the phonon-related part of the low-energy Hamiltonian in Eq. (15)], it is given by

$$\begin{aligned}\hat{\mathcal{H}} &= \sum_l g^{(p)}(n_l-\langle n_l\rangle)x_l + \sum_l\frac{1}{2}(\omega^{(p)})^2x_l^2 \\ &= \sum_l g^{(p)}n_l x_l + \sum_l\frac{1}{2}(\omega^{(p)})^2\left(x_l-x_l^0\right)^2 + \text{const.},\end{aligned} \tag{41}$$

where $x_l^0 = g^{(p)}\langle n_l\rangle/(\omega^{(p)})^2$. In the above expression, we take the atomic mass to be 1, for simplicity. Now the physical meaning of the double-counting correction becomes clear: It gives the shift of the potential minimum of the lattice vibration by x_l^0, which is proportional to the occupation of the electron $\langle n_l\rangle$. x_l^0 gives the equilibrium position of the lattice vibration without the effect of the low-energy electron manifold. When we solve the model at the mean-field (DFT) level, the equilibrium position goes back to the optimized position within the DFT, since the contributions from Eqs. (39) and (40) cancel each other.

E. Comparison between our scheme and the scheme proposed in Ref. [59]

Recently, Giovannetti *et al.* [59] also proposed a downfolding scheme for electron-phonon-coupled systems. Here, we compare our scheme with that of Giovannetti *et al.* The main difference is the form of the double-counting correction. In Ref. [59], the phonon-related part of the Hamiltonian [64], which corresponds to Eq. (41) in our case, is given by

$$\begin{aligned}\hat{\mathcal{H}} &= \sum_l g^{(p)}x_l^0 n_l + \sum_l g^{(p)}n_l\left(x_l-x_l^0\right) \\ &\quad + \sum_l\frac{1}{2}(\omega^{(p)})^2\left(x_l-x_l^0\right)^2.\end{aligned} \tag{42}$$

Here, the electron-phonon coupling $g^{(p)}$ is calculated at $x_l = x_l^0$, while in our scheme $g^{(p)}$ is calculated at $x_l=0$. Furthermore, Giovannetti *et al.* include the term $\sum_l g^{(p)}x_l^0 n_l$, which represents the deformation of the band due to the difference in the equilibrium position between that in the low-energy Hamiltonian and that obtained by the DFT optimization. Thus, Giovannetti *et al.* also introduce the correction to the electronic part, while our scheme only includes the correction to phonons. Therefore, the form of the Hamiltonian in Ref. [59] is more general than ours.

If the difference in the equilibrium position is large (i.e., $|x_l^0|$ is large), the band deformation term $\sum_l g^{(p)} x_l^0 n_l$ will become important. In the case of fullerides, which are discussed in the next section, we conclude that this effect is small because the equilibrium positions of the undoped and doped C_{60} solids are very similar, which makes the effect of doping an almost-rigid band shift. Thus, our scheme is indeed applicable to the fulleride problem. However, of course, there exist systems in which this band deformation effect is significant. Reference [59] argues that it is important to take into account the band deformation effect in the case of the K-doped picene system [65], because the deformation of the molecule by doping is not negligible.

To derive the parameters in Eq. (42), Giovannetti *et al.* assume that the electrons couple to a single optical phonon, while in our scheme, we can treat all phonon modes. First, Giovannetti *et al.* estimate $g^{(p)}$ by calculating the electron-phonon coupling for the undoped picene system. Then they determine x_l^0 and $\omega^{(p)}$ such that the mean-field solution of the Hamiltonian recovers the equilibrium positions and the phonon frequencies of the doped system derived within the DFT and DFPT.

We still lack the methodology to derive a Hamiltonian with the form of Eq. (42) in a totally *ab initio* way, i.e., without simplifying the electron-phonon coupling or determining x_l^0 and $\omega^{(p)}$ in the postprocessing. To realize this, we need to develop an *ab initio* structure optimization scheme without the effect of low-energy electrons. We also have to carefully consider the change in electronic parameters. When we derive a model based on the optimized structure without the effect of low-energy electrons, for example, the shape of the Wannier function can be different from that with the fully optimized structure. Then the values of Coulomb interaction parameters can differ from those with the conventional cRPA, which uses the Wannier functions constructed from the fully optimized structure. When band deformation is really severe, we might have to be careful in the choice of the low-energy subspace since the low-energy band character of the optimized structure without the effect of low-energy electrons might change from that of the fully optimized structure. Therefore, there remain many open questions and challenges regarding the derivation of a Hamiltonian including the band deformation term [Eq. (42)]. Note that, in the situation where this band deformation is important, the cDFPT is also challenged, since the current cDFPT does not take account of its effect.

IV. APPLICATION

A. Calculation conditions

We performed cDFPT calculations [51] for five fcc A_3C_{60} systems, namely, K_3C_{60}, Rb_3C_{60}, and Cs_3C_{60} with three different lattice parameters, whose properties are summarized in Table I. We employed the same lattice constants as those employed in Ref. [66] to evaluate the Coulomb parameters by the cRPA. We specify the material by the volume ($V_{C_{60}^{3-}}$) occupied per C_{60}^{3-} anion in a solid. The most expanded material (Cs_3C_{60}, with $V_{C_{60}^{3-}} = 804$ Å^3) is a Mott insulator and the second most expanded system (Cs_3C_{60}, with $V_{C_{60}^{3-}} =$ 784 Å^3) is on the verge of the metal-insulator transition [67]. The other three materials show a metallic behavior and the superconductivity emerges at low temperatures.

TABLE I. List of materials employed in the calculation. We list the name of compounds, the lattice constant a, the corresponding volume occupied per C_{60}^{3-} anion in a solid, the applied pressure in experiments, and the superconducting transition temperature T_c or Néel temperature T_N. Listed materials are the same as those in Ref. [66] (in Ref. [66], the Coulomb interaction parameters and hopping parameters are evaluated).

	a (Å)	$V_{C_{60}^{3-}}$ (Å^3)	Pressure (kb)	T_c (T_N) (K)	Ref. No.
fcc K_3C_{60}	14.240	722	0	19	[68]
fcc Rb_3C_{60}	14.420	750	0	29	[68]
fcc Cs_3C_{60}	14.500	762	7	35	[67]
fcc Cs_3C_{60}	14.640	784	2	26	[67]
fcc Cs_3C_{60}	14.762	804	0	(2.2)	[67]

As explained in Sec. III, the implementation of the cDFPT can be done by slightly modifying the existing DFPT program. Among the various DFPT codes, in the present study, we modified the one implemented in the QUANTUM ESPRESSO package [61,62] (see Appendix C). In the cDFPT calculation, we need to define the low-energy subspace (t subspace). Figure 1 shows the band structure for fcc Cs_3C_{60} with $V_{C_{60}^{3-}} =$ 762 Å^3. Around the Fermi level, there exist the so-called t_{1u} bands originating from threefold degenerate LUMO orbitals of the C_{60} molecule. The t_{1u} bands are isolated from other bands. As mentioned in Sec. I, the low-energy physics is governed by low-energy bands, therefore, we choose the t_{1u} bands as target bands.

The phonon calculations with the cDFPT and the DFPT were performed after the DFT ground-state calculations. In the DFT part, we adopted the local density approximation with the Perdew-Zunger parametrization [69]. The

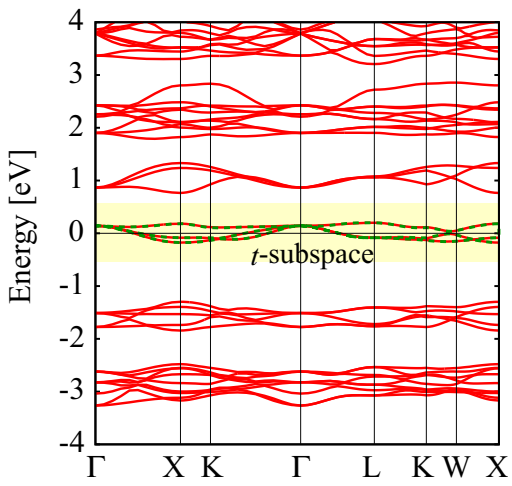

FIG. 1. (Color online) DFT band structure of fcc Cs_3C_{60} with $V_{C_{60}^{3-}} = 762$ Å^3. We choose the t_{1u} bands as the t subspace [shaded (yellow) region]. Dotted (green) curves denote the band dispersion derived by Wannier hopping parameters for the t subspace.

TABLE II. Partially renormalized phonon frequencies of H_g modes at the Γ point calculated by the cDFPT method, in cm^{-1} (1 eV = 8065.54 cm^{-1}). In I_h symmetry (molecular limit), the H_g-mode phonon frequencies are fivefold degenerate. In fcc A_3C_{60} systems, they are split into threefold degenerate and twofold degenerate frequencies due to the crystal field. Thus, we list two frequencies for each H_g mode. We list the values of $V_{C_{60}{}^{3-}}$ (in $Å^3$) in parentheses just after the material names in column headings.

	Frequency (cm^{-1})				
Mode	K_3C_{60} (722)	Rb_3C_{60} (750)	Cs_3C_{60} (762)	Cs_3C_{60} (784)	Cs_3C_{60} (804)
$H_g(1)$	260, 271	258, 269	259, 278	259, 274	258, 272
$H_g(2)$	433, 435	433, 433	434, 436	434, 435	433, 435
$H_g(3)$	706, 708	707, 708	709, 710	709, 710	709, 710
$H_g(4)$	785, 786	785, 787	787, 797	786, 793	785, 791
$H_g(5)$	1124, 1128	1124, 1129	1129, 1138	1127, 1135	1126, 1132
$H_g(6)$	1282, 1287	1282, 1287	1292, 1298	1288, 1294	1286, 1291
$H_g(7)$	1451, 1455	1452, 1455	1463, 1466	1459, 1461	1457, 1459
$H_g(8)$	1563, 1564	1563, 1565	1573, 1573	1569, 1570	1567, 1568

pseudopotentials for C, K, Rb, and Cs atoms were prepared using the same procedure as in Ref. [70] (Troullier-Martins norm-conserving pseudopotentials [71] in the Kleinman-Bylander representation [72]). We employed a $4 \times 4 \times 4$ **k** mesh and a cutoff energy of 50 Ry for wave functions. Under the above conditions, we performed the structure optimization for the materials listed in Table I by fixing the lattice constant and ignoring the orientational disorder. In the phonon calculation part, we employed a $2 \times 2 \times 2$ **q** mesh and a Gaussian smearing of 0.025 Ry.

B. Phonon frequencies

In alkali-doped fullerides, it has been shown that the dominant electron-phonon coupling comes from the intramolecular vibration [53,74–79]. When we consider the isolated C_{60} molecule, only intramolecular phonon modes with A_g and H_g symmetries have finite electron-phonon couplings to t_{1u} electrons [80,81]. This is because the C_{60} molecule has extremely high symmetry (I_h symmetry), and coupling to the other modes is forbidden due to the symmetry [53]. This property also holds well in C_{60} solids. In particular, coupling to the Jahn-Teller phonon (so-called H_g modes) is argued to be crucial to the superconductivity [13,82].

Table II summarizes our calculated partially renormalized phonon frequencies ($\omega^{(p)}$'s) of H_g modes at the Γ point. Due to the crystal field, the frequencies of H_g modes are split in two. The high phonon frequencies, up to ∼1600 cm^{-1} (∼0.2 eV), can be ascribed to the stiff C-C bonds and the lightness of carbon atoms. Furthermore, the intramolecular nature of the modes leads to the following features: The H_g phonon modes have little dispersion (see Fig. 2). The material dependence of the frequencies is weak.

Note that these partially renormalized frequencies $\omega^{(p)}$ are the inputs for the low-energy solvers and thus cannot be directly compared with the experimentally observed frequencies. To compare with experiments, we have to include the effect of t-subspace electrons and calculate the fully renormalized phonon frequencies ($\omega^{(f)}$). In general, a stronger coupling between t-subspace electrons and phonons leads to a larger difference between $\omega^{(p)}$'s and $\omega^{(f)}$'s [50]. In the case of alkali-doped fullerides, the electron-phonon coupling of the individual mode is not large, while the accumulation of contributions leads to a total electron-phonon coupling of $\lambda \sim 0.5-1.0$ [6–8,82]. Therefore, we do not expect a large difference between $\omega^{(p)}$'s and $\omega^{(f)}$'s.

In Table III, we list the fully renormalized phonon frequencies of H_g modes at the Γ point computed by the DFPT.

TABLE III. Fully renormalized phonon frequencies of H_g modes at the Γ point calculated by the conventional DFPT method, in cm^{-1} (1 eV = 8065.54 cm^{-1}). The splitting of the frequencies of each H_g mode is due to the crystal field. We list the values of $V_{C_{60}{}^{3-}}$ (in $Å^3$) in parentheses just after the material names in column headings. For comparison, we also show the experimentally observed phonon frequencies in K_3C_{60} [73].

	Frequency (cm^{-1})					
Mode	K_3C_{60} (722)	Rb_3C_{60} (750)	Cs_3C_{60} (762)	Cs_3C_{60} (784)	Cs_3C_{60} (804)	K_3C_{60} (expt.)[a]
$H_g(1)$	257, 268	255, 267	256, 277	255, 273	255, 271	271
$H_g(2)$	423, 425	422, 423	422, 425	421, 424	420, 423	431
$H_g(3)$	683, 686	684, 686	686, 688	686, 688	686, 687	723
$H_g(4)$	777, 778	777, 778	780, 788	779, 785	778, 782	...
$H_g(5)$	1110, 1114	1110, 1114	1116, 1125	1113, 1121	1112, 1118	...
$H_g(6)$	1267, 1273	1267, 1272	1277, 1283	1273, 1278	1270, 1275	...
$H_g(7)$	1402, 1407	1403, 1405	1415, 1415	1410, 1410	1406, 1407	1408
$H_g(8)$	1531, 1536	1531, 1535	1541, 1544	1537, 1540	1535, 1538	1547

[a]Raman scattering measurement from Ref. [73].

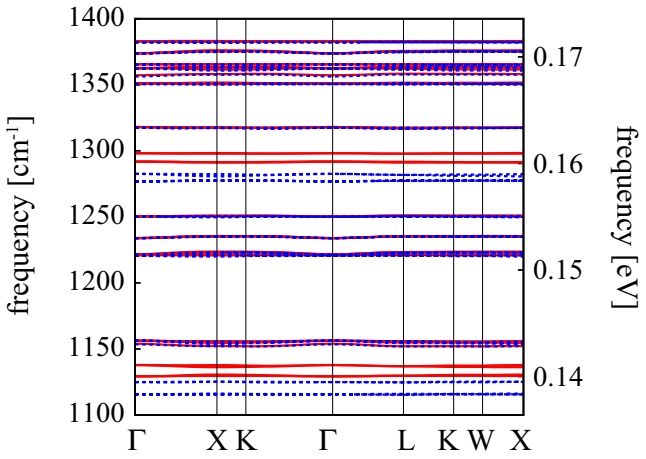

FIG. 2. (Color online) Phonon dispersion of fcc Cs_3C_{60} with $V_{C_{60}^{3-}} = 762$ Å^3. For the sake of visibility, we restrict the frequency range to 1100–1400 cm^{-1}. Solid (red) curves indicate partially renormalized frequencies calculated by the cDFPT; dotted (blue) curves, fully renormalized frequencies calculated by the conventional DFPT.

By comparing them with the partially renormalized values in Table II, we see the softening of frequencies. This is because the phonons are dressed by the coupling between phonons and t_{1u} electrons. In other words, phonons acquire the self-energy associated with t-subspace electrons. However, as expected (see the discussion above), the difference is small: The absolute difference is at most $\sim$50 cm^{-1}. If we consider the ratio $\omega^{(f)}/\omega^{(p)}$, it exceeds 0.95; i.e., the difference is less than 5%. Even when we accurately treat the t-subspace processes beyond the DFPT level by the model-calculation method, the t-subspace renormalization effects will remain small. Then we can expect that conventional DFPT calculations give reasonable estimates of the phonon frequencies. Indeed, the fully renormalized frequencies in Table III agree well with the experimental data [73,83].

Figure 2 shows both the partially [solid (red) lines] and the fully [dotted (blue) lines] renormalized phonon frequencies between 1100 and 1400 cm^{-1} for fcc Cs_3C_{60} with $V_{C_{60}^{3-}} = 762$ Å^3. Several intramolecular modes including H_g modes [$H_g(5)$ and $H_g(6)$] and non-H_g modes exist in this frequency range. While they are common in that they have few dispersions, we see a clear difference between the H_g modes and the others in the way of softening: Non-H_g modes do not couple to t_{1u} electrons [84]. Hence, their frequencies are not affected by the inclusion of t-subspace renormalization effects. As a result, the dotted (blue) curves ($\omega^{(f)}$) are on top of the solid (red) curves ($\omega^{(p)}$) for non-H_g modes. On the other hand, the frequencies for H_g modes are renormalized by a few percent. Indeed, the red and blue curves are located at different positions for H_g modes (see the frequency regions 1100–1150 and 1260–1300 cm^{-1}).

C. Phonon-mediated effective interactions between low-energy electrons

If we write down the partition function for the electron-phonon-coupled Hamiltonian, Eq. (15), in the coherent-state path-integral formalism, we find that we have at most a quadratic term for the phonon fields. Then we can integrate out the phonon degrees of freedom analytically. This results in an electronic model with an additional electron-electron interaction mediated by phonons (Fig. 3) [85], whose on-site (=intramolecular) part $V^{(p)}_{ij,i'j'}(i\omega_n)$ is given by [51]

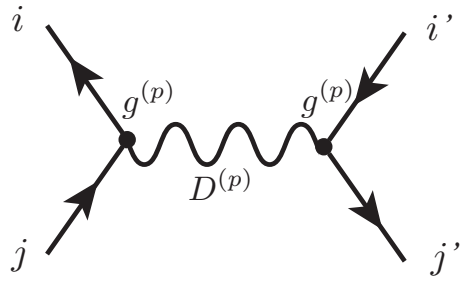

FIG. 3. Feynman diagram of phonon-mediated interaction between electrons. Solid lines with arrows represent the electron propagator; wavy line, the phonon propagator; and filled circles, the electron-phonon coupling.

$$V^{(p)}_{ij,i'j'}(i\omega_n) = \frac{1}{N_{\mathbf{q}}}\sum_{\mathbf{q}\nu} \tilde{g}^{(p)}_{ij}(\mathbf{q},\nu)\, D^{(p)}_{\mathbf{q},\nu}(i\omega_n)\, \tilde{g}^{(p)*}_{j'i'}(\mathbf{q},\nu)$$
$$= -\frac{1}{N_{\mathbf{q}}}\sum_{\mathbf{q}\nu} \tilde{g}^{(p)}_{ij}(\mathbf{q},\nu)\, \frac{2\omega^{(p)}_{\mathbf{q}\nu}}{\omega_n^2 + \left(\omega^{(p)}_{\mathbf{q}\nu}\right)^2}\, \tilde{g}^{(p)*}_{j'i'}(\mathbf{q},\nu), \tag{43}$$

where $N_{\mathbf{q}}$ is the number of the $\mathbf{q}$ mesh and ω_n is the bosonic Matsubara frequency $\omega_n = 2\pi nT$ with the temperature T [86]. Here, $\tilde{g}^{(p)}$'s are given by

$$\tilde{g}^{(p)}_{ij}(\mathbf{q},\nu) = \frac{1}{N_{\mathbf{k}}}\sum_{\mathbf{k}} g^{(p)\nu}_{ij}(\mathbf{k},\mathbf{q}). \tag{44}$$

Here, the partially screened electron-phonon coupling $g^{(p)}$ is used to calculate the phonon-mediated interactions. In Appendix E, we discuss that the vertex correction for $g^{(p)}$ is small, which makes the estimate of the phonon-mediated interactions without the vertex correction reliable.

Phonon-mediated interactions $V^{(p)}_{ij,i'j'}(i\omega_n)$ are dynamical interactions, which vanish in the high-frequency limit ($\omega_n \to \infty$). We call the intraorbital density-density-type, interorbital density-density-type, and exchange-type interactions $U^{(p)}_{\rm ph}(i\omega_n)$, $U'^{(p)}_{\rm ph}(i\omega_n)$, and $J^{(p)}_{\rm ph}(i\omega_n)$, respectively; i.e.,

$$\begin{aligned} U^{(p)}_{\rm ph}(i\omega_n) &= V^{(p)}_{ii,ii}(i\omega_n), \\ U'^{(p)}_{\rm ph}(i\omega_n) &= V^{(p)}_{ii,jj}(i\omega_n), \\ J^{(p)}_{\rm ph}(i\omega_n) &= V^{(p)}_{ij,ji}(i\omega_n) = V^{(p)}_{ij,ij}(i\omega_n), \end{aligned} \tag{45}$$

with $i \neq j$. We also define the fully screened quantities $U^{(f)}_{\rm ph}(i\omega_n)$, $U'^{(f)}_{\rm ph}(i\omega_n)$, and $J^{(f)}_{\rm ph}(i\omega_n)$ in the same way; i.e., $U^{(f)}_{\rm ph}(i\omega_n) = V^{(f)}_{ii,ii}(i\omega_n)$, $U'^{(f)}_{\rm ph}(i\omega_n) = V^{(f)}_{ii,jj}(i\omega_n)$, and $J^{(f)}_{\rm ph}(i\omega_n) = V^{(f)}_{ij,ji}(i\omega_n) = V^{(f)}_{ij,ij}(i\omega_n)$. We find that, because of the high symmetry of the t_{1u} orbitals, the values of $U^{(p,f)}_{\rm ph}(i\omega_n)$, $U'^{(p,f)}_{\rm ph}(i\omega_n)$, and $J^{(p,f)}_{\rm ph}(i\omega_n)$ do not depend on the orbital.

TABLE IV. Material dependence of the static part ($\omega_n = 0$) of the effective intramolecular interactions mediated by phonons. Values in parentheses just after material names in column headings denote $V_{C_{60}{}^{3-}}$ (in Å^3).

Type of	Interaction (meV)				
interaction	K_3C_{60} (722)	Rb_3C_{60} (750)	Cs_3C_{60} (762)	Cs_3C_{60} (784)	Cs_3C_{60} (804)
$U_{\rm ph}^{(p)}(0)$	−152	−142	−114	−124	−134
$U_{\rm ph}^{\prime(p)}(0)$	−53	−42	−13	−22	−31
$J_{\rm ph}^{(p)}(0)$	−50	−51	−51	−51	−52
$U_{\rm ph}^{(f)}(0)$	−73	−74	−73	−74	−75
$U_{\rm ph}^{\prime(f)}(0)$	28	29	30	31	31
$J_{\rm ph}^{(f)}(0)$	−51	−52	−52	−52	−53

Table IV summarizes the values of the static parts of these interactions ($\omega_n = 0$). We find that the relation $U_{\rm ph}^{\prime(p,f)}(0) \sim U_{\rm ph}^{(p,f)}(0) - 2J_{\rm ph}^{(p,f)}(0)$ holds well and also holds for finite frequencies (see Fig. 4). We first discuss partially renormalized interactions. The negative values of $U_{\rm ph}^{(p)}(0)$, $U_{\rm ph}^{\prime(p)}(0)$, and $J_{\rm ph}^{(p)}(0)$ indicate that the interactions are attractive at $\omega_n = 0$. Therefore, they will compete with the repulsive on-site Coulomb interactions. As for the density-density channel, since the intramolecular Coulomb repulsion (Hubbard U) for t_{1u} electrons is estimated to be of the order of $\sim$1 eV [66], the repulsive Coulomb interaction dominates over the phonon-mediated attraction. However, remarkably, the situation changes for the exchange-type interaction: the absolute value of $|J_{\rm ph}^{(p)}(0)| \sim 0.05$ eV is larger than that of the Hund's coupling, $J \sim 0.035$ eV [66]. Therefore, in fullerides, an effectively negative exchange interaction is realized [13]. This is contrast with, e.g., the case of LaFeAsO (the first discovered iron-based superconductor [87]), where the Hund's coupling is as large as $\sim$0.5 eV [25,88] and the phonon-mediated exchange interaction, $J_{\rm ph}^{(p)}(0) \sim -0.02$, eV gives only a minor correction [51]. The unusual competition of the Hund's coupling and the phonon-mediated interactions can be ascribed, mainly, to the following two factors [13]. One is the molecular nature of the maximally localized Wannier orbitals. Thus, the sizes of Wannier orbitals become larger than those of atomic-orbital-like Wannier functions, which results in a smaller Hund's coupling. The other is the enhancement of the negative $J_{\rm ph}^{(p)}(0)$ due to the strong couplings between Jahn-Teller modes and t_{1u} electrons. Jahn-Teller H_g modes give the non-density-type electron-phonon coupling, which contributes to $J_{\rm ph}^{(p)}(0)$ [80,81,89]. Note that non-Jahn-Teller A_g modes do not contribute, since the couplings of A_g modes are of the density type.

As for the material dependence, while that of $J_{\rm ph}^{(p)}(0)$ is small, we see discernible material dependence in $U_{\rm ph}^{(p)}(0)$ and $U_{\rm ph}^{\prime(p)}(0)$. We identify the origin of the material dependence to be the vibration modes of alkali ions at tetrahedral sites. It is reasonable that they make a material-dependent contribution as the distances between $C_{60}{}^{3-}$ anions and/or alkali cations change. Indeed, if we compute $U_{\rm ph}^{(p)}(0)$ and $U_{\rm ph}^{\prime(p)}(0)$ for the five materials excluding the alkali-ion contributions (in this case, the values become the sum of the contributions from intramolecular phonons), the results for $U_{\rm ph}^{(p)}(0)$ [$U_{\rm ph}^{\prime(p)}(0)$] are, in ascending order of $V_{C_{60}{}^{3-}}$, −89 meV [10], −91 meV [9], −91 meV [9], −93 meV [8], and −95 meV [8]. As is clear, they have much less material dependence than those with alkali-ion contributions, which is natural because we would expect that intramolecular phonons have little material dependence. We find that the alkali-ion modes couple to the total density of t_{1u} electrons; i.e., they couple to the density of the individual orbital with almost the same amplitudes ($\tilde{g}_{11}^{(p)} \simeq \tilde{g}_{22}^{(p)} \simeq \tilde{g}_{33}^{(p)}$). Thus, it does not contribute to $J_{\rm ph}^{(p)}$. The contribution to $J_{\rm ph}^{(p)}(0)$ originates from the intramolecular Jahn-Teller coupling (coupling to H_g modes). Therefore, we see little material dependence of $J_{\rm ph}^{(p)}(0)$. Since the electron-phonon coupling of the alkali-ion modes are of the density type, the alkali-ion mode contribution is efficiently screened by t_{1u} electrons, which leads to a minor role of the alkali-ion modes in superconductivity. As a result, as we see below, the dominant contribution to fully renormalized interactions comes from intramolecular phonons, which is consistent with previous studies [75,90].

We can compute the fully screened phonon-mediated on-site interactions using Eq. (43) by replacing the partially renormalized quantities with the fully renormalized quantities. We list the values of their static part ($\omega_n = 0$) in Table IV. We find that the magnitudes of density-density-type interactions, $U_{\rm ph}^{\prime(f)}(0)$ and $U_{\rm ph}^{(f)}(0)$, differ substantially from those of partially renormalized ones, $U_{\rm ph}^{\prime(p)}(0)$ and $U_{\rm ph}^{(p)}(0)$. On the other hand, the values of $J_{\rm ph}^{(f)}(0)$ are almost unchanged from those of $J_{\rm ph}^{(p)}(0)$. This different behavior of $U_{\rm ph}$, $U'_{\rm ph}$, and $J_{\rm ph}$ can be understood as follows. t_{1u} electrons efficiently screen non-Jahn-Teller-type electron-phonon coupling but not Jahn-Teller-type coupling. The former contributes to $U_{\rm ph}$ and $U'_{\rm ph}$. Therefore, the difference between the partially and the fully renormalized quantities is substantial. On the other hand, only the Jahn-Teller phonon contributes to $J_{\rm ph}$. Therefore, we have little difference between the partially and the fully renormalized quantities. As we discuss above, the alkali-ion-mode contribution becomes small in the fully renormalized quantities and the intramolecular H_g-mode contribution becomes dominant (the intramolecular A_g-mode contribution is also screened because A_g modes couple to the total density of t_{1u} electrons), which makes the material dependence of $U_{\rm ph}^{(f)}(0)$, $U_{\rm ph}^{\prime(f)}(0)$, and $J_{\rm ph}^{(f)}(0)$ small.

When we consider the contribution from H_g modes in the molecular limit [80,81,89], we can show that the relation

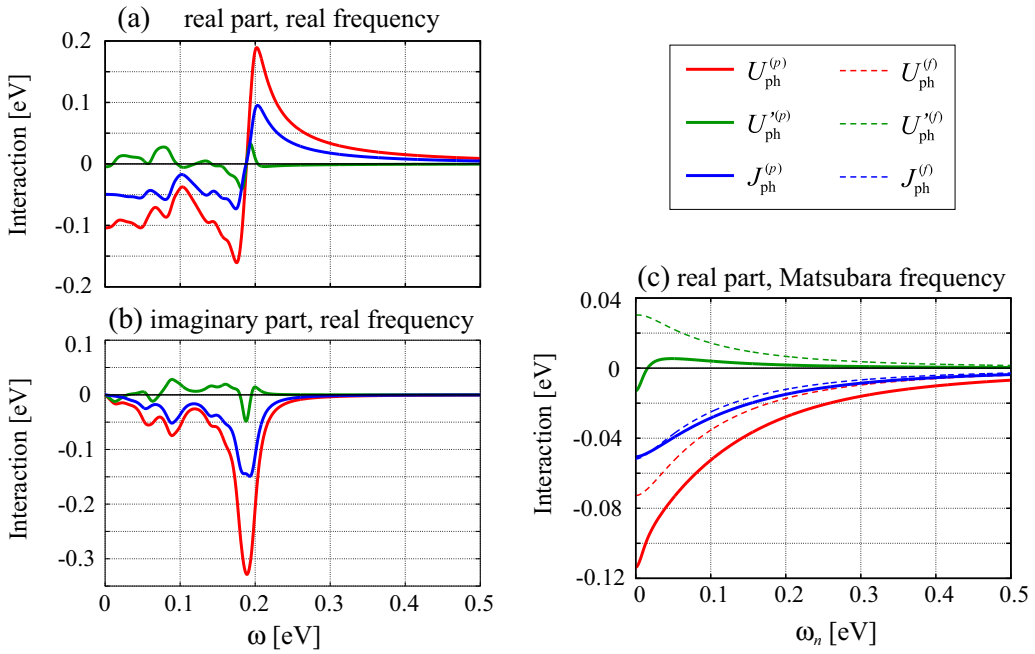

FIG. 4. (Color online) Frequency dependence of phonon-mediated interactions for fcc Cs_3C_{60} with $V_{C_{60}^{3-}} = 762$ Å^3 (a, b) along the real frequency and (c) along the Matsubara axis. (a) Real and (b) imaginary part of $U_{ph}^{(p)}(\omega)$, $U_{ph}^{\prime(p)}(\omega)$, and $J_{ph}^{(p)}(\omega)$. The frequency dependences of these quantities are calculated at $\omega + i\eta$ with $\eta = 0.01$ eV. (c) Real part of $U_{ph}^{(p)}(i\omega_n)$, $U_{ph}^{\prime(p)}(i\omega_n)$, $J_{ph}^{(p)}(i\omega_n)$, $U_{ph}^{(f)}(i\omega_n)$, $U_{ph}^{\prime(f)}(i\omega_n)$, and $J_{ph}^{(f)}(i\omega_n)$. The imaginary part is always 0 along the Matsubara axis.

$U_{ph}^{\prime(f)}(i\omega_n) = -U_{ph}^{(f)}(i\omega_n)/2$ holds. Since, in reality, we have a small contribution from the other modes such as A_g and the alkali-ion modes, the above relation does not exactly hold. However, this naturally explains why the interorbital interactions become repulsive ($U_{ph}^{\prime(f)}(0) > 0$).

We, finally, discuss the frequency dependence of phonon-mediated interactions. The frequency dependences for fcc Cs_3C_{60} with $V_{C_{60}^{3-}} = 762$ Å^3 on the real-frequency axis are shown in Figs. 4(a) and 4(b), which illustrate the real and the imaginary parts of phonon-mediated interactions, respectively. Since the frequencies of intramolecular phonons range up to ∼0.2 eV, there exist significant structures below ∼0.2 eV. Im $U_{ph}^{(p)}(\omega)$ and Im $J_{ph}^{(p)}(\omega)$ are always negative. On the other hand, Im $U_{ph}^{\prime(p)}(\omega)$ can be both negative and positive. This is because the contributions from the non-Jahn-Teller and the Jahn-Teller (H_g) phonons coexist [the former (latter) makes a negative (positive) contribution]. Note that both non-Jahn-Teller and Jahn-Teller phonons make a negative contribution to Im$U_{ph}^{(p)}(\omega)$ and Im$J_{ph}^{(p)}(\omega)$.

We also show the frequency dependence along the Matsubara frequencies in Fig. 4(c), where we also plot the frequency dependence of fully screened interactions. Again, the nonmonotonic behavior of $U_{ph}^{\prime(p)}(i\omega_n)$ can be ascribed to the coexistence of attractive (non-Jahn-Teller) and repulsive (Jahn-Teller) contributions. Because the contribution from non-Jahn-Teller phonons becomes small in fully screened interactions, the frequency dependence of $U_{ph}^{\prime(f)}(i\omega_n)$ becomes monotonic. Since only Jahn-Teller modes, which are poorly screened by t_{1u} electrons, contribute to J_{ph}, we have a small difference between $J_{ph}^{(p)}(i\omega_n)$ and $J_{ph}^{(f)}(i\omega_n)$. Finally, we note that the relation $U_{ph}^{\prime(p,f)} = U_{ph}^{(p,f)} - 2J_{ph}^{(p,f)}$ holds well along both the real and the imaginary frequency axes.

V. CONCLUSION AND OUTLOOK

In this paper, we have presented a detailed explanation of a newly developed *ab initio* downfolding scheme for the electron-phonon-coupled system, the cDFPT. With the cDFPT, we can calculate the partially renormalized phonon frequencies and electron-phonon coupling, which are used as the parameters in the effective low-energy Hamiltonian. We have shown that the cDFPT scheme can be easily implemented by a slight modification of the conventional DFPT scheme.

We have applied the cDFPT scheme to alkali-doped fullerides. By excluding the t-subspace renormalization effect, we have seen hardening of the frequencies of phonon modes which couple to t-subspace electrons. We have also discussed the difference between partially and fully screened phonon-mediated interactions. In partially screened interactions, non-Jahn-Teller phonons make substantial contributions. However, in fully screened screened interactions, the contribution from non-Jahn-Teller modes becomes small because it is efficiently screened by t_{1u} electrons. Thus, Jahn-Teller phonons make the dominant contributions to fully screened interactions.

In this paper, we have focused on alkali-doped fullerides. However, in principle, the cDFPT is applicable to other materials in which phonons play a crucial role. These applications remain interesting and important future issues. There also remain challenges on the developmenal side: As discussed

in Sec. III E, the current cDFPT is not applicable when the equilibrium positions of the ions are changed drastically by coupling to low-energy electrons. It is also challenged when there exists strong anharmonicity in the system. These are important open questions in the downfolding for electron-phonon-coupled systems.

ACKNOWLEDGMENTS

We would like to thank Kazuma Nakamura, Shiro Sakai, Massimo Capone, Ryosuke Akashi, Takahiro Ohgoe, Terumasa Tadano, Masatoshi Imada, Atsushi Fujimori, Atsushi Oshiyama, and Yoshihiro Iwasa for fruitful discussions. Y.N. was supported by Grant-in-Aid for JSPS Fellows No. 12J08652 from the Japan Society for the Promotion of Science (JSPS).

APPENDIX A: EQUIVALENCE OF EQS. (6) AND (8)

Here, we show that Eqs. (6) and (8) indeed give the same solution. When we write Eq. (8) as

$$\underbrace{(\mathcal{H}_{\rm SCF}+Q-\varepsilon_n)}_{A}\underbrace{|\Delta\psi_n\rangle}_{\mathbf{x}}=\underbrace{-(\tilde{\theta}_{F,n}-P_n)\Delta V_{\rm SCF}|\psi_n\rangle}_{\mathbf{y}}, \quad \text{(A1)}$$

the A matrix is given, in the Bloch basis (note that, in the case of QUANTUM ESPRESSO, the plane basis is used in the actual calculation), by

$$A=\begin{pmatrix} \varepsilon_1+\alpha_1-\varepsilon_n & & & 0 \\ & \varepsilon_2+\alpha_2-\varepsilon_n & & \\ & & \ddots & \\ 0 & & & \varepsilon_M+\alpha_M-\varepsilon_n \end{pmatrix}, \quad \text{(A2)}$$

where M is the size of the basis set describing the Bloch states. $\tilde{\theta}_{F,n}-P_n$, on the r.h.s of Eq. (8), is rewritten as

$$\begin{aligned}\tilde{\theta}_{F,n}-P_n &= \sum_m\left[\tilde{\theta}_{F,n}\left(1-\tilde{\theta}_{n,m}\right)-\tilde{\theta}_{F,m}\tilde{\theta}_{m,n}-\alpha_m\frac{\tilde{\theta}_{F,n}-\tilde{\theta}_{F,m}}{\varepsilon_n-\varepsilon_m}\tilde{\theta}_{m,n}\right]|\psi_m\rangle\langle\psi_m| \\ &= \sum_m\left[\left(\tilde{\theta}_{F,n}-\tilde{\theta}_{F,m}\right)\tilde{\theta}_{m,n}-\alpha_m\frac{\tilde{\theta}_{F,n}-\tilde{\theta}_{F,m}}{\varepsilon_n-\varepsilon_m}\tilde{\theta}_{m,n}\right]|\psi_m\rangle\langle\psi_m| \\ &= -\sum_m\left[\frac{\tilde{\theta}_{F,n}-\tilde{\theta}_{F,m}}{\varepsilon_n-\varepsilon_m}\tilde{\theta}_{m,n}(\varepsilon_m+\alpha_m-\varepsilon_n)\right]|\psi_m\rangle\langle\psi_m|. \end{aligned} \quad \text{(A3)}$$

With Eqs. (A1), (A2), and (A3), we can show that $|\Delta\psi_n\rangle$ is given by

$$|\Delta\psi_n\rangle=A^{-1}\mathbf{y}=\sum_m\frac{\tilde{\theta}_{F,n}-\tilde{\theta}_{F,m}}{\varepsilon_n-\varepsilon_m}\tilde{\theta}_{m,n}|\psi_m\rangle\langle\psi_m|\Delta V_{\rm SCF}|\psi_n\rangle, \quad \text{(A4)}$$

which is nothing but a proof that Eq. (8) gives the same result as Eq. (6).

APPENDIX B: COMPARISON BETWEEN THE cDFPT AND THE cRPA

Here, we compare the present cDFPT with the cRPA [23]. In the cRPA, which derives the effective electron-electron interactions in the low-energy model, we calculate the partially screened Coulomb interaction as [23]

$$W^{(p)}=\left(1-v\chi_r^0\right)^{-1}v. \quad \text{(B1)}$$

The fully screened Coulomb interaction is obtained by further taking into account the t-subspace screening effect:

$$W^{(f)}=\left(1-W^{(p)}\chi_t^0\right)^{-1}W^{(p)}. \quad \text{(B2)}$$

One can see that Eqs. (B1) and (B2) have the same structure as the screened electron-phonon coupling [Eqs. (30) and (31)]. Both the cRPA and the cDFPT methods rely on the same kind of decomposition of the screening processes. In both cases, we calculate the partially screened quantities, which are to be used in the low-energy Hamiltonian.

APPENDIX C: PRACTICAL IMPLEMENTATION IN THE CASE OF QUANTUM ESPRESSO

Here, we provide an example of how we modify a source code. In the DFPT implemented in version 4.3.1 of QUANTUM ESPRESSO [61,62], the $\beta_{n,m}$ parameters are defined in "orthogonalize.f90," which exists in the "PH" folder. In Ref. [91], we distribute a modified "orthogonalize.f90" under the GNU General Public License [92].

APPENDIX D: CONFIRMATION OF THE EQUALITY $\Sigma = \Sigma_t + \Sigma_r$ IN SEC. III B

Here, we show that the equality $\Sigma = \Sigma_t + \Sigma_r$ in Sec. III B indeed holds. In principle, the self-energy Σ, the electron-phonon coupling g, the polarization function χ^0, and so on, are expressed as matrices. In this section, for the sake of simplicity, we treat them as if they were scalar quantities. One can easily extend the proof to the case where they are matrices. $\Sigma_t = |g^{(p)}|^2 \chi^t_{\rm DFT}$ is rewritten as

$$\begin{aligned}
\Sigma_t &= |g^{(p)}|^2 \frac{\chi_t^0}{1-\tilde{W}^{(p)}\chi_t^0} \\
&= |g^{(b)}|^2 \frac{1}{1-\tilde{v}\chi_r^0}\frac{\chi_t^0}{1-\tilde{W}^{(p)}\chi_t^0}\frac{1}{1-\tilde{v}\chi_r^0} \\
&= |g^{(b)}|^2 \left(1+\frac{\tilde{v}\chi_r^0}{1-\tilde{v}\chi_r^0}\right)\frac{\chi_t^0}{1-\tilde{W}^{(p)}\chi_t^0}\left(1+\frac{\tilde{v}\chi_r^0}{1-\tilde{v}\chi_r^0}\right) \\
&= |g^{(b)}|^2 \left(1+\chi_r^0\tilde{W}^{(p)}\right)\frac{\chi_t^0}{1-\tilde{W}^{(p)}\chi_t^0}\left(1+\tilde{W}^{(p)}\chi_r^0\right) \\
&= |g^{(b)}|^2 \left[\frac{\chi_t^0}{1-\tilde{W}^{(p)}\chi_t^0} + \chi_r^0\frac{\tilde{W}^{(p)}}{1-\tilde{W}^{(p)}\chi_t^0}\chi_t^0 + \chi_t^0\frac{\tilde{W}^{(p)}}{1-\tilde{W}^{(p)}\chi_t^0}\chi_r^0 + \chi_r^0\tilde{W}^{(p)}\frac{\chi_t^0}{1-\tilde{W}^{(p)}\chi_t^0}\tilde{W}^{(p)}\chi_r^0 \right] \\
&= |g^{(b)}|^2 \left[\chi_t^0 + \chi_t^0\tilde{W}^{(f)}\chi_t^0 + \chi_r^0\tilde{W}^{(f)}\chi_t^0 + \chi_t^0\tilde{W}^{(f)}\chi_r^0 + \chi_r^0\tilde{W}^{(p)}\frac{\chi_t^0}{1-\tilde{W}^{(p)}\chi_t^0}\tilde{W}^{(p)}\chi_r^0 \right].
\end{aligned} \tag{D1}$$

Similarly, $\Sigma_r = |g^{(b)}|^2 \chi^r_{\rm DFT}$ is rewritten as

$$\Sigma_r = |g^{(b)}|^2 \frac{\chi_r^0}{1-\tilde{v}\chi_r^0} = |g^{(b)}|^2 \left[\, \chi_r^0 + \chi_r^0\tilde{W}^{(p)}\chi_r^0 \,\right]. \tag{D2}$$

Using the equality

$$\tilde{W}^{(p)} + \tilde{W}^{(p)}\frac{\chi_t^0}{1-\tilde{W}^{(p)}\chi_t^0}\tilde{W}^{(p)} = \frac{\tilde{W}^{(p)}}{1-\tilde{W}^{(p)}\chi_t^0} = \tilde{W}^{(f)}, \tag{D3}$$

one can show that $\Sigma_t + \Sigma_r$ is expressed as

$$\begin{aligned}
\Sigma_t + \Sigma_r &= |g^{(b)}|^2 \left[\, \chi_t^0 + \chi_r^0 + \left(\chi_t^0 + \chi_r^0\right)\tilde{W}^{(f)}\left(\chi_t^0 + \chi_r^0\right) \,\right] \\
&= |g^{(b)}|^2 \left[\, \chi^0 + \chi^0\tilde{W}^{(f)}\chi^0 \,\right] \\
&= |g^{(b)}|^2 \chi_{\rm DFT},
\end{aligned} \tag{D4}$$

which agrees with the expression for Σ in Eq. (33).

APPENDIX E: SMALLNESS OF THE ELECTRON-PHONON VERTEX CORRECTION IN THE DOWNFOLDING PROCEDURE

Due to the high phonon frequency, ∼0.1 eV, which is comparable to the typical electronic kinetic energy, ∼0.5 eV, the Migdal theorem [93] is violated in A_3C_{60} systems. Therefore, we need a careful consideration of the vertex corrections. In this Appendix, we argue that, as far as processes involving high-energy electrons are concerned, the electron-phonon vertex corrections are small.

To see this, let us consider the "first-order" vertex correction diagram in Fig. 5. For simplicity, we assume that the multiple intramolecular phonon modes are represented by a single Einstein phonon branch with frequency ω_0 and that the electron-phonon vertex g has no momentum dependence (or the electron-phonon coupling is local). Then the inclusion of the diagram in Fig. 5 gives the correction to the bare electron-phonon vertex g_0 as $g_0 \to g_0(1+\gamma)$, with γ being a dimensionless quantity given by

$$\gamma = -\frac{T}{N_{\mathbf{k}}}\sum_{k'} g_1 g_2 D(k-k')G(k')G(k'+q), \tag{E1}$$

where the g_i's, D, and G are the dressed electron-phonon vertices, phonon Green's function, and electron Green's function, respectively. The g_i's and G have orbital indices, while we do not show them, for simplicity. k [q] represents a set of the momentum and the fermionic [bosonic] Matubara frequency, $k = (\mathbf{k}, \nu_n)$ [$q = (\mathbf{q}, \omega_n)$]. T is the temperature and $N_{\mathbf{k}}$ is the number of $\mathbf{k}$ points. Note that this diagram is of first order with respect to D, however, it contains higher order diagrams with respect to the bare phonon Green's function D_0. In the downfolding procedure, low-energy processes are excluded, therefore, the two-electron Green's function in Eq. (E1) should be a combination of G_H and G_H or of G_H and G_L, where G_H (G_L) is the propagator of the high-energy (low-energy) electrons [94]. Then the typical order of γ associated with the

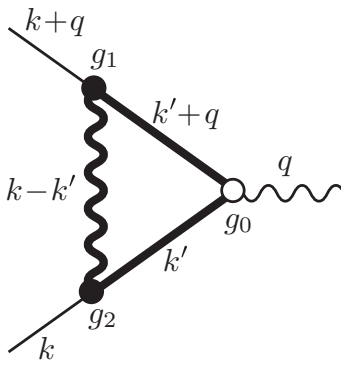

FIG. 5. First-order electron-phonon vertex correction diagram. The open (filled) circle represents the bare (dressed) electron-phonon coupling. The thick (thin) solid and wavy lines indicate dressed (bare) electron and phonon propagators, respectively.

downfolding is given by $|\gamma| \sim 2g_1g_2/\omega_r \times 1/\Delta E$ with the renormalized phonon frequency ω_r and the typical particle-hole excitation energy scale involving high-energy degrees of freedom ΔE. Here, to derive this expression, we have employed the fact that the typical order of the convolution of G_H and G_H or G_H and G_L is $\sim 1/\Delta E$. In the case of alkali-doped fullerides, ΔE is at least $\sim$1 eV. $2g_1g_2/\omega_r$ is nothing but the static part of the fully screened phonon-mediated interaction. If g_1 and g_2 are the coupling between phonons and low-energy electrons, it corresponds to $U_{\rm ph}^{(f)}(0)$, $U_{\rm ph}^{\prime(f)}(0)$, and $J_{\rm ph}^{(f)}(0)$ in Table. IV. While we do not estimate the coupling between phonons and high-energy electrons, we expect the order of the phonon-mediated interactions involving high-energy electrons to be the same as that of $U_{\rm ph}^{\prime(f)}(0)$ and $J_{\rm ph}^{(f)}(0)$. In addition, in the diagrams considered in the downfolding procedure, the orbital indices for g_1 and g_2 are usually different. This is because one is the coupling to the electron state and the other is the coupling to the hole state, which would make $2g_1g_2/\omega_r$ smaller. In any case, $2g_1g_2/\omega_r$ will be, at most, $\sim$0.1 eV. As a result, the correction γ associated with the downfolding will take a small value, $\gamma < 0.1$.

In conclusion, the neglect of electron-phonon vertex corrections in the model-derivation step as in the case of the cDFPT is justified. However, we note that we still need a careful treatment for vertex corrections in the model-analysis step since vertex corrections in the t subspace are not negligible any more.

[1] Z.-X. Shen, A. Lanzara, S. Ishihara, and N. Nagaosa, Philos. Mag. Part B **82**, 1349 (2002).
[2] F. Giustino, M. L. Cohen, and S. G. Louie, Nature (London) **452**, 975 (2008).
[3] O. Gunnarsson and O. Rösch, J. Phys.: Condens. Matter **20**, 043201 (2008).
[4] D. Reznik, G. Sangiovanni, O. Gunnarsson, and T. P. Devereaux, Nature (London) **455**, E6 (2008).
[5] S. Johnston, F. Vernay, B. Moritz, Z.-X. Shen, N. Nagaosa, J. Zaanen, and T. P. Devereaux, Phys. Rev. B **82**, 064513 (2010).
[6] N. Iwahara, T. Sato, K. Tanaka, and L. F. Chibotaru, Phys. Rev. B **82**, 245409 (2010).
[7] J. Laflamme Janssen, M. Côté, S. G. Louie, and M. L. Cohen, Phys. Rev. B **81**, 073106 (2010).
[8] C. Faber, J. L. Janssen, M. Côté, E. Runge, and X. Blase, Phys. Rev. B **84**, 155104 (2011).
[9] Z. P. Yin, A. Kutepov, and G. Kotliar, Phys. Rev. X **3**, 021011 (2013).
[10] R. Akashi and R. Arita, Phys. Rev. Lett. **111**, 057006 (2013).
[11] R. Akashi and R. Arita, J. Phys. Soc. Jpn. **83**, 061016 (2014).
[12] R. Akashi, M. Kawamura, S. Tsuneyuki, Y. Nomura, and R. Arita, Phys. Rev. B **91**, 224513 (2015).
[13] Y. Nomura, S. Sakai, M. Capone, and R. Arita, Sci. Adv. **1**, e1500568 (2015).
[14] M. Capone, M. Fabrizio, C. Castellani, and E. Tosatti, Science **296**, 2364 (2002).
[15] M. Capone, M. Fabrizio, C. Castellani, and E. Tosatti, Rev. Mod. Phys. **81**, 943 (2009).
[16] J. E. Han, O. Gunnarsson, and V. H. Crespi, Phys. Rev. Lett. **90**, 167006 (2003).
[17] G. Kotliar, S. Y. Savrasov, K. Haule, V. S. Oudovenko, O. Parcollet, and C. A. Marianetti, Rev. Mod. Phys. **78**, 865 (2006).
[18] K. Held, Adv. Phys. **56**, 829 (2007).
[19] M. Imada and T. Miyake, J. Phys. Soc. Jpn. **79**, 112001 (2010).
[20] N. Marzari and D. Vanderbilt, Phys. Rev. B **56**, 12847 (1997).
[21] I. Souza, N. Marzari, and D. Vanderbilt, Phys. Rev. B **65**, 035109 (2001).
[22] N. Marzari, A. A. Mostofi, J. R. Yates, I. Souza, and D. Vanderbilt, Rev. Mod. Phys. **84**, 1419 (2012).
[23] F. Aryasetiawan, M. Imada, A. Georges, G. Kotliar, S. Biermann, and A. I. Lichtenstein, Phys. Rev. B **70**, 195104 (2004).
[24] K. Nakamura, R. Arita, and H. Ikeda, Phys. Rev. B **83**, 144512 (2011).
[25] T. Miyake, K. Nakamura, R. Arita, and M. Imada, J. Phys. Soc. Jpn. **79**, 044705 (2010).
[26] M. Aichhorn, L. Pourovskii, V. Vildosola, M. Ferrero, O. Parcollet, T. Miyake, A. Georges, and S. Biermann, Phys. Rev. B **80**, 085101 (2009).
[27] Z. P. Yin, K. Haule, and G. Kotliar, Nat. Phys. **7**, 294 (2011).
[28] T. Misawa, K. Nakamura, and M. Imada, J. Phys. Soc. Jpn. **80**, 023704 (2011).
[29] T. Misawa and M. Imada, Nat. Commun. **5**, 5738 (2014).
[30] H. Sakakibara, H. Usui, K. Kuroki, R. Arita, and H. Aoki, Phys. Rev. Lett. **105**, 057003 (2010).
[31] L. de' Medici, X. Wang, M. Capone, and A. J. Millis, Phys. Rev. B **80**, 054501 (2009).
[32] C. Weber, K. Haule, and G. Kotliar, Phys. Rev. B **82**, 125107 (2010).
[33] P. Hansmann, N. Parragh, A. Toschi, G. Sangiovanni, and K. Held, New J. Phys. **16**, 033009 (2014).
[34] I. A. Nekrasov, G. Keller, D. E. Kondakov, A. V. Kozhevnikov, T. Pruschke, K. Held, D. Vollhardt, and V. I. Anisimov, Phys. Rev. B **72**, 155106 (2005).
[35] A. Georges, L. d. Medici, and J. Mravlje, Annu. Rev. Condens. Matter Phys. **4**, 137 (2013).
[36] K. Nakamura, Y. Yoshimoto, T. Kosugi, R. Arita, and M. Imada, J. Phys. Soc. Jpn. **78**, 083710 (2009).
[37] H. Shinaoka, T. Misawa, K. Nakamura, and M. Imada, J. Phys. Soc. Jpn. **81**, 034701 (2012).
[38] M. Hirayama, T. Miyake, and M. Imada, Phys. Rev. B **87**, 195144 (2013).
[39] A. van Roekeghem, T. Ayral, J. M. Tomczak, M. Casula, N. Xu, H. Ding, M. Ferrero, O. Parcollet, H. Jiang, and S. Biermann, Phys. Rev. Lett. **113**, 266403 (2014).
[40] Y. Nomura, M. Kaltak, K. Nakamura, C. Taranto, S. Sakai, A. Toschi, R. Arita, K. Held, G. Kresse, and M. Imada, Phys. Rev. B **86**, 085117 (2012).
[41] A. Kutepov, K. Haule, S. Y. Savrasov, and G. Kotliar, Phys. Rev. B **82**, 045105 (2010).
[42] M. Kinza and C. Honerkamp, Phys. Rev. B **92**, 045113 (2015).
[43] P. Werner, M. Casula, T. Miyake, F. Aryasetiawan, A. J. Millis, and S. Biermann, Nature Phys. **8**, 331 (2012).

[44] L. Huang and Y. Wang, EPL (Europhys. Lett.) **99**, 67003 (2012).

[45] H. Shinaoka, M. Troyer, and P. Werner, Phys. Rev. B **91**, 245156 (2015).

[46] J. M. Tomczak, M. Casula, T. Miyake, and S. Biermann, Phys. Rev. B **90**, 165138 (2014).

[47] J. M. Tomczak, M. Casula, T. Miyake, F. Aryasetiawan, and S. Biermann, EPL (Europhys. Lett.) **100**, 67001 (2012).

[48] R. Sakuma, P. Werner, and F. Aryasetiawan, Phys. Rev. B **88**, 235110 (2013).

[49] C. Taranto, M. Kaltak, N. Parragh, G. Sangiovanni, G. Kresse, A. Toschi, and K. Held, Phys. Rev. B **88**, 165119 (2013).

[50] J. Bauer, J. E. Han, and O. Gunnarsson, Phys. Rev. B **84**, 184531 (2011).

[51] Y. Nomura, K. Nakamura, and R. Arita, Phys. Rev. Lett. **112**, 027002 (2014).

[52] A. F. Hebard, M. J. Rosseinsky, R. C. Haddon, D. W. Murphy, S. H. Glarum, T. T. M. Palstra, A. P. Ramirez, and A. R. Kortan, Nature **350**, 600 (1991).

[53] O. Gunnarsson, Rev. Mod. Phys. **69**, 575 (1997).

[54] R. H. Zadik, Y. Takabayashi, G. Klupp, R. H. Colman, A. Y. Ganin, A. Potočnik, P. Jeglič, D. Arčon, P. Matus, K. Kamarás *et al.*, Sci. Adv. **1**, e1500059 (2015).

[55] P. Giannozzi, S. de Gironcoli, P. Pavone, and S. Baroni, Phys. Rev. B **43**, 7231 (1991).

[56] S. de Gironcoli, Phys. Rev. B **51**, 6773 (1995).

[57] F. Favot and A. Dal Corso, Phys. Rev. B **60**, 11427 (1999).

[58] S. Baroni, S. de Gironcoli, A. Dal Corso, and P. Giannozzi, Rev. Mod. Phys. **73**, 515 (2001).

[59] G. Giovannetti, M. Casula, P. Werner, F. Mauri, and M. Capone, Phys. Rev. B **90**, 115435 (2014).

[60] The derivation of Eq. (4) relies on the fact that the ionic potential is local, i.e., depends on only one electronic coordination **r**. In actual calculations using the pseudopotentials, the ionic potential usually contains nonlocal components, terms which depend on two electronic coordinations, **r** and **r**′. See Ref. [58] for the expression of interatomic force constants in the presence of nonlocal components. However, the presence of nonlocal components does not change the outline of the paper at all.

[61] P. Giannozzi, S. Baroni, N. Bonini, M. Calandra, R. Car, C. Cavazzoni, D. Ceresoli, G. L. Chiarotti, M. Cococcioni, I. Dabo *et al.*, J. Phys.: Condens. Matter **21**, 395502 (2009).

[62] http://www.quantum-espresso.org/.

[63] Strictly speaking, this expression [Eq. (24)] is valid only when the ionic potential $V_{\rm ion}$ is purely local. In practice, we employ the pseudopotential, which has a nonlocal part. In this case, one has to introduce three-point response functions in the formulation, however, it does not change the outline presented in this section.

[64] In Ref. [59], the Hamiltonian also includes the electron one-body and cRPA Coulomb interaction terms.

[65] R. Mitsuhashi, Y. Suzuki, Y. Yamanari, H. Mitamura, T. Kambe, N. Ikeda, H. Okamoto, A. Fujiwara, M. Yamaji, N. Kawasaki, Y. Maniwa, and Y. Kubozono, Nature **464**, 76 (2010).

[66] Y. Nomura, K. Nakamura, and R. Arita, Phys. Rev. B **85**, 155452 (2012).

[67] A. Y. Ganin, Y. Takabayashi, P. Jeglič, D. Arčon, A. Potočnik, P. J. Baker, Y. Ohishi, M. T. McDonald, M. D. Tzirakis, A. McLennan *et al.*, Nature (London) **466**, 221 (2010).

[68] O. Zhou and D. E. Cox, J. Phys. Chem. Solids **53**, 1373 (1992).

[69] J. P. Perdew and A. Zunger, Phys. Rev. B **23**, 5048 (1981).

[70] R. Akashi and R. Arita, Phys. Rev. B **88**, 054510 (2013).

[71] N. Troullier and J. L. Martins, Phys. Rev. B **43**, 1993 (1991).

[72] L. Kleinman and D. M. Bylander, Phys. Rev. Lett. **48**, 1425 (1982).

[73] P. Zhou, K.-A. Wang, A. M. Rao, P. C. Eklund, G. Dresselhaus, and M. S. Dresselhaus, Phys. Rev. B **45**, 10838 (1992).

[74] C. Christides, D. A. Neumann, K. Prassides, J. R. D. Copley, J. J. Rush, M. J. Rosseinsky, D. W. Murphy, and R. C. Haddon, Phys. Rev. B **46**, 12088 (1992).

[75] V. P. Antropov, O. Gunnarsson, and A. I. Liechtenstein, Phys. Rev. B **48**, 7651 (1993).

[76] W. Pickett, D. Papaconstantopoulos, M. Pederson, and S. Erwin, J. Superconduct. **7**, 651 (1994).

[77] T. Ebbesen, J. Tsai, K. Tanigaki, H. Hiura, Y. Shimakawa, Y. Kubo, I. Hirosawa, and J. Mizuki, Physica C: Superconduc. **203**, 163 (1992).

[78] B. Burk, V. H. Crespi, M. Fuhrer, A. Zettl, and M. L. Cohen, Physica C: Superconduct. **235-240**, 2493 (1994).

[79] B. Burk, V. H. Crespi, A. Zettl, and M. L. Cohen, Phys. Rev. Lett. **72**, 3706 (1994).

[80] C. M. Varma, J. Zaanen, and K. Raghavachari, Science **254**, 989 (1991).

[81] M. Lannoo, G. A. Baraff, M. Schlüter, and D. Tomanek, Phys. Rev. B **44**, 12106 (1991).

[82] O. Gunnarsson, *Alkali-Doped Fullerides: Narrow-Band Solids with Unusual Properties* (World Scientific, Singapore, 2004).

[83] D. S. Bethune, G. Meijer, W. C. Tang, H. J. Rosen, W. G. Golden, H. Seki, C. A. Brown, and M. S. de Vries, Chem. Phys. Lett. **179**, 181 (1991).

[84] The two A_g modes can couple to t_{1u} electrons, however, they do not exist in this range; the experimentally observed frequencies are 496 and 1470 $\rm cm^{-1}$ [83].

[85] F. F. Assaad and T. C. Lang, Phys. Rev. B **76**, 035116 (2007).

[86] In principle, the sum over ν in Eq. (43) runs from 1 to 189. However, we omit the contribution from the lowest nine branches ($\nu = 1-9$). They correspond to the acoustic modes, librations, and alkali-ion vibrations at octahedral sites. [70] Within the present calculation, some of these vibrations have imaginary frequencies. The neglect can be justified since the couplings between these modes and t_{1u} electrons are small [53,82].

[87] Y. Kamihara, T. Watanabe, M. Hirano, and H. Hosono, J. Am. Chem. Soc. **130**, 3296 (2008).

[88] K. Nakamura, R. Arita, and M. Imada, J. Phys. Soc. Jpn. **77**, 093711 (2008).

[89] O. Gunnarsson, Phys. Rev. B **51**, 3493 (1995).

[90] O. Gunnarsson and G. Zwicknagl, Phys. Rev. Lett. **69**, 957 (1992).

[91] http://qe-forge.org/gf/project/cdfpt/frs/.

[92] http://www.gnu.org/licenses/gpl-3.0.en.html.

[93] A. B. Migdal, Sov. Phys. JETP **7**, 996 (1958).

[94] If the off-diagonal Green's function $G_{\rm HL}$ is nonzero, we also have to take into account the processes involving $G_{\rm HL}$. However, the off-diagonal Green's functions are usually very small compared to the diagonal ones, thus the effects of $G_{\rm HL}$ on the vertex correction γ are small.